EXPERIMENTAL STUDIES ON FREE JET OF MATCH ROCKETS AND UNSTEADY FLOW OF HOUSEFLIES

by

Angel David Lozano Galarza

A Thesis

Submitted to the Faculty of Purdue University

In Partial Fulfillment of the Requirements for the degree of

Master of Science in Interdisciplinary Engineering

Department of Mechanical and Civil Engineering

Hammond, Indiana

May 2021

THE PURDUE UNIVERSITY GRADUATE SCHOOL
STATEMENT OF COMMITTEE APPROVAL

Dr. Yun Liu, Chair

Mechanical and Civil Engineering Department

Dr. Nuri Zeytinoglu

Mechanical and Civil Engineering Department

Dr. Ran Zhou

Mechanical and Civil Engineering Department

Dr. Xiuling Wang

Mechanical and Civil Engineering Department

Approved by:

Dr. Nesrin Ozalp

ACKNOWLEDGMENTS

First, I would like to express my sincere gratitude to my mentor, Prof. Yun Liu for his support and guidance throughout this research. During these two year, he has encouraged me to be part of different projects to expand my knowledge of fluid mechanics and learn valuable things. It was a great honor to meet and work with him.

Also, I would like to thank my parents and little sister for their love, care and support when times I needed them the most. My parents have always been there for me with their wisdom and advises to guide me in every step of my education.

TABLE OF CONTENTS

LIST OF FIGURES

ABSTRACT

The aerodynamics of insect flight is not well understood despite it has been extensively investigated with various techniques and methods. Its complexities mainly have two folds: complex flow behavior and intricate wing morphology. The complex flow behavior in insect flight are resulted from flow unsteadiness and three-dimensional effects. However, most of the experimental studies on insect flight were performed with 2D flow measurement techniques whereas the 3D flow measurement techniques are still under developing. Even with the most advanced 3D flow measurement techniques, it is still impossible to measure the flow field closed to the wings and body. On the other hand, the intricate wing morphology complicates the experimental studies with mechanical flapping wings and make mechanical models difficult to mimic the flapping wing motion of insects. Therefore, to understand the authentic flow phenomena and associated aerodynamics of insect flight, it is inevitable to study the actual flying insects.

In this thesis, a recently introduced technique of schlieren photography is first tested on free jet of match rockets with a physics based optical flow method to explore its potential of flow quantification of unsteady flow. Then the schlieren photography and optical flow method are adapted to tethered and feely flying houseflies to investigate the complex wake flow and structures. In the end, a particle tracking velocimetry system: Shake the Box system, is utilized to resolve the complex wake flow on a tethered house fly and to acquire some preliminary 3D flow field data

1. INTRODUCTION

1.1 Background Overview

Flapping flight involves complex locomotion movements and complex flow phenomenon while the animal is hovering, taking off, and landing. Flow on flapping wings is highly unsteady and three-dimensional compared with fixed wings, where the flow can be considered approximately steady and two-dimensional. For example, an insect to support its body weight must produce 2–3 times more lift than can be accounted for with conventional aerodynamic theories while having incredible maneuverability with quick accelerations (Ellington C. P., 1999). The unsteady aerodynamic flight of insects is usually characterized by large-scale vortex structures, complicated flapping-wing kinematics, and flexible wing structures (Liu & Aono, 2009). A flapping cycle can be divided into four stages: two translational phases (upstroke and downstroke), when the wings sweep through the air with a high angle of attack, and two rotational phases (pronation and supination), when the wings rapidly rotate and reverse direction (Dickinson, Lehmann, & Sane, 1999). A deep understanding of the aerodynamics of flapping wings is crucial to comprehend the flight behavior of more than a million insect species and approximately eleven thousand vertebrates (Chin & Lentink, 2016).

The well-known story of ‘bumblebee cannot fly’ can be traced back to 1919 when Hoff suggested that animals flew with the aerodynamics of fixed wings (Bomphrey, Taylor, & Thomas, 2009). In addition, in 1934, August Magnan and André Sainte-Lague concluded that bees' flight was impossible when fixed-wing aircraft theories were applied (McMasters, 1989; Douglas L. Altshuler, Vance, Roberts, & Dickinson, 2005). They modeled bumblebee wings as a pair of flat plates traveling through the air. Therefore, the insects flap their wings at high angles of attack (AoA), resulting in flow separation and high drag and low lift production, something that is not desired in conventional fixed wings, which operate at low angles of attack. Moreover, the Kutta condition no longer applies as the viscous flow structures shed and become highly unsteady around the wing.

In 1996, Ellington experimented on a tethered hawkmoth and visualized leading-edge vortex structures on the wings (LEV) (Ellington, Berg, Willmott, & Thomas, 1996). The structure of LEV is considered as one major mechanism of lift augmentation and accounted for 2/3 of the total lift production on hovering insects (Muijres, et al., 2008). Although, this explained how augmented lift is produced, it raised more questions about the LEV and the unsteady aerodynamics of flapping wings. Consequently, flapping wing aerodynamics has gathered a lot of interest among researchers and scientists in studying lift generation mechanisms on some vertebrates such as hummingbirds, bats, and owls. As well as on different insects, including the fruit fly, bumblebee, hawkmoth, rhinoceros beetle, cicada, and mosquito

(Oh, Lee, Park, Choi, & Kim, 2019). Due to the difficulties in capturing and measuring the flow field close to the wings, even though all of these studies have contributed to the understanding of flapping wing aerodynamics, there still not a clear understanding about the flow structures and their associated unsteady aerodynamics. Moreover, most aerodynamic researches have focused on medium and large size insects. While on small insects, studies have been conducted with dynamic-scaled mechanical models that mimic the flapping wing motion. In this study, two state-of-the-art approaches (Schlieren photography and Particle-Tracking-Velocimetry) are implemented to capture the near-body flow structure and resolve the three-dimensional flow field on tethered houseflies.

1.2 Aerodynamic Theory of Insect Flight

Understanding aerodynamic forces generation on insects are essential to biologists and engineers to comprehend animal locomotion and aerodynamics. On flying insects, one critical mechanism for lift augmentation is the attached leading-edge vortex (LEV) (Figure 1.1. Ellington, Berg, Willmott, & Thomas, 1996; Berg & Ellington, 1997). The LEV is formed when insects flap their wings at high angles of attack and flow separates from the leading edge. Then separation layer rolls up, creating the LEV and it remains attached to the wing until it is shed at the end of each half-stroke during reversals. This ability of staying attached can help the flow to conform Kutta condition and avoids stall, thereby increasing the lift generation. In addition, drag is also increased and insects use the increased drag to initiate acceleration into forward or backward flight (Ellington C. P., 1999). This flow structure has been identified in different researches and on different insect species, but the mechanics to stabilize it are stilled under investigation and study (Liu & Aono, 2009). Other aerodynamic mechanisms include added mass, rotational circulation, clap and fling, and wing–wake interactions (in Figure 1.2). The added mass takes into consideration of the acceleration of the wing and the acceleration of the fluid around the wing. This increases the pressure on the wing, and the effect can be interpreted as additional mass on the wings. On the other hand, the rotational circulation takes place during the rotational/stroke reversal phase. When the wing rotates and translates the Kutta condition fails, an additional circulation is created and augments the lift production (Jardin, Chatellier, Farcy, & David, 2009). Depending on the timings of duration and rotation t (relative to wing stroke), it can enhance or attenuate the force generated during the translation phase (Chin & Lentink, 2016).

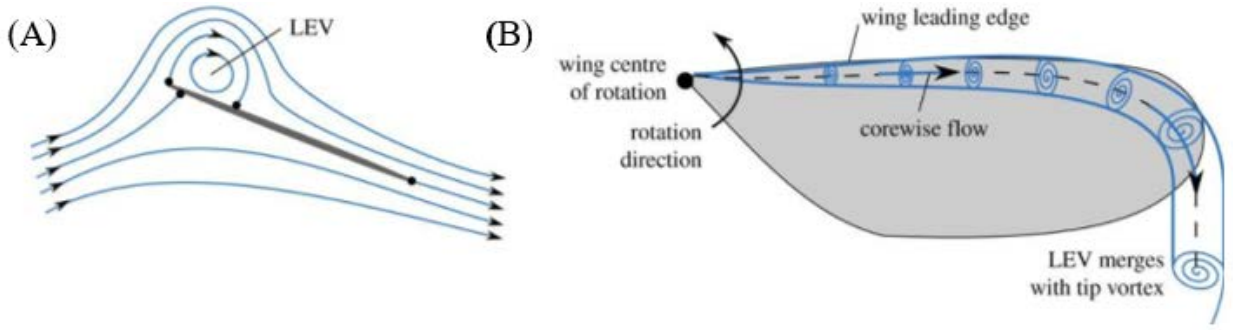

Figure 1. 1 Formation of the leading-edge vortex (LEV). (A) Fulfillment of the Kutta condition in insects at high angles of attack. (B) Topology of the LEV. (Nabawy & Crowther 2017).

The clap and fling mechanism, also known as Weis-Fogh mechanism, references to the wing motion, the "clap" when the wings meet, and the "fling" when they apart. During the "clap," vorticity is shed by the trailing edges as they get together, forming a stopping vortex and the opposite circulation sign of each wing cancels out. This annulate the Wagner effect, and circulation can build up much faster, extending lift over subsequent strokes. Also, the little gap between the wings pushes fluid out, producing thrust. During the "fling," as the wing separates from each other, fluid fills the empty space providing an increase in circulation. (Lehmann, Sane, & Dickinson, The aerodynamic effects of wing–wing interaction in flapping insect wings, 2005). Although this mechanism enhances lift production, many species do not use it or rarely use it, only under specific circumstances: during take-off, carrying loads, and making sharp turns (Chin & Lentink, 2016). In the mechanism of wing-wake interaction, when an insect starts a new stroke, its wings reverse direction and encounter the wake generated from the previous strokes, resulting in higher relative velocities and aerodynamic force production (Jardin, Chatellier, Farcy, & David, 2009). Furthermore, flying insects operate over a broad range of Reynolds numbers from approximately 10 to 10^4; for comparison, a swimming human has a Reynolds number of 10^6 (Sane, 2003). Therefore, insects operate at much lower Re and viscous effect plays a vital role on its flow physics and associated aerodynamics (Sane, 2003).

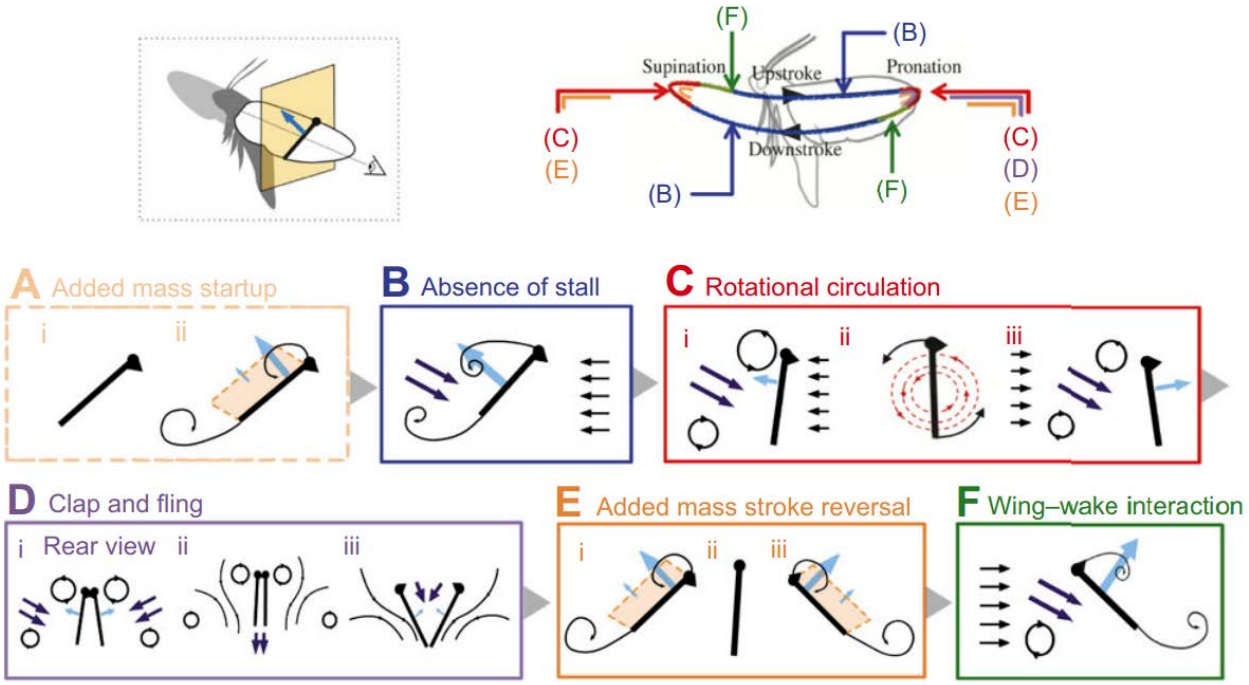

Figure 1. 2 (Top) Insect wing kinematics. (A-F) Black arrows indicate airflow direction, and light blue arrows represent net forces. (A) Added mass sequence. (i) wing starts acceleration (ii) pressure increases around the wing, adding mass (shaded region). (B) Formation of the LEV that prevents stall and increases lift augmentation. (C) Additional circulation is generated during supination and pronation, known as the Kramer effect, which increases lift production. The wing is shown (i) before, (ii) during, (iii) after rotation. (D) Clap and fling sequence. (i) When the wings meet 'clap', opposing circulations cancel out. (ii) The close gap between the wings pushes fluid out, producing thrust. (iii) During the 'fling', when the wings get away from each other and translation begins, new fluid rushes in and speeds up circulation generation. (E) Added mass effect as the wing (i) decelerates for (ii) rotation and (iii) accelerates for translation. (F) Wing interaction with the wake generated during the previous stroke. (Chin & Lentink, 2016).

1.3 Experimental Challenges

In the light of CFD simulation, particle velocimetry (including PIV and PTV), and other flow visualization techniques, the complex flow on flying animals have been extensively investigated and studied. However, most of the studies have been performed on medium or large size insects, whereas the flow on small insects is difficult to study with. Moreover, as insect wingbeat frequency increases as size decrease, fruit fly flaps its wings at a flapping frequency of about 200 Hz (Sane, 2003). These two factors, including small size and high flapping frequency, lead to most studies on small insects being conducted on mechanical flappers that can mimic the complex wing motion/kinematics or in CFD simulations.

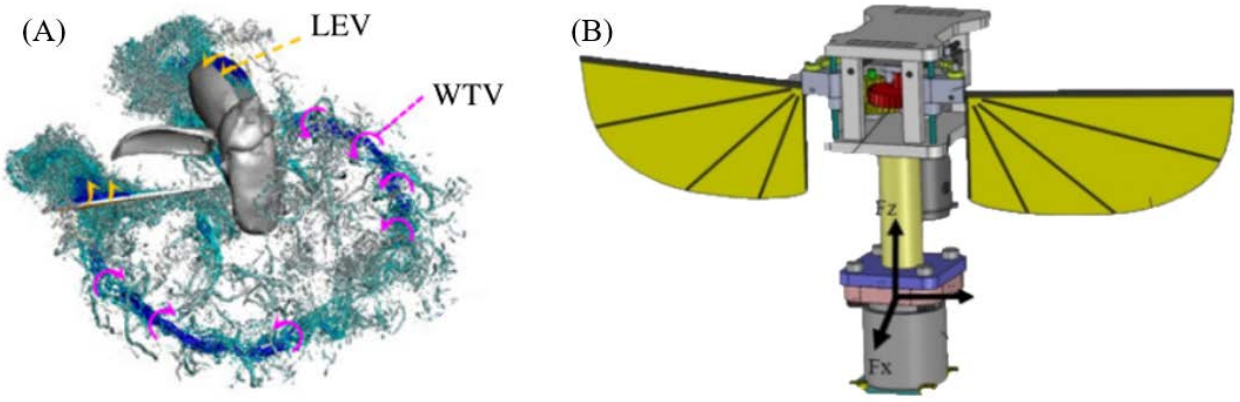

Figure 1. 3. (A) Numerical Simulation of a hovering rhinoceros beetle (*Trypoxylus dichotomus*) showing the leading-edge vortex (LEV) and wing-tip vortex (WTV) (Oh, Lee, Park, Choi, & Kim, 2019). (B) Mechanical flapper that reproduces camber and twisting deformation (Truong, Nguyen, & Lee, 2017).

Digital Particle Image Velocimetry (DPIV) is extensively implemented to quantify the flow field from capturing images of tracer particles. Then the particle images can be correlated with computational algorithms to derive 2D displacement/velocity field. 2D PIV has been widely implemented to study different flow phenomena, including the flow field on flying insects. However, on small insects, particle seeding and laser intensity is an issue that leads the insect to not cooperate, even with tethered insects (Lehmann, 2012). On the other hand, Tomographic PIV uses several cameras to record a volume of tracer particles from different angles, enabling reconstructing 3D flow field. This technique has been implemented on a tethered locust, showing interesting flow structures, but it was limited only to the far-field away from the insect. (Henningsson, et al., 2015). In addition, just to process the data set from one complete wingbeat cycle, it took 96 days with a 48-multicore processor. Moreover, the setup consisted of eight high-resolution and high-sensitivity cameras and a powerful laser, making the cost a considerable challenge to replicate in other labs.

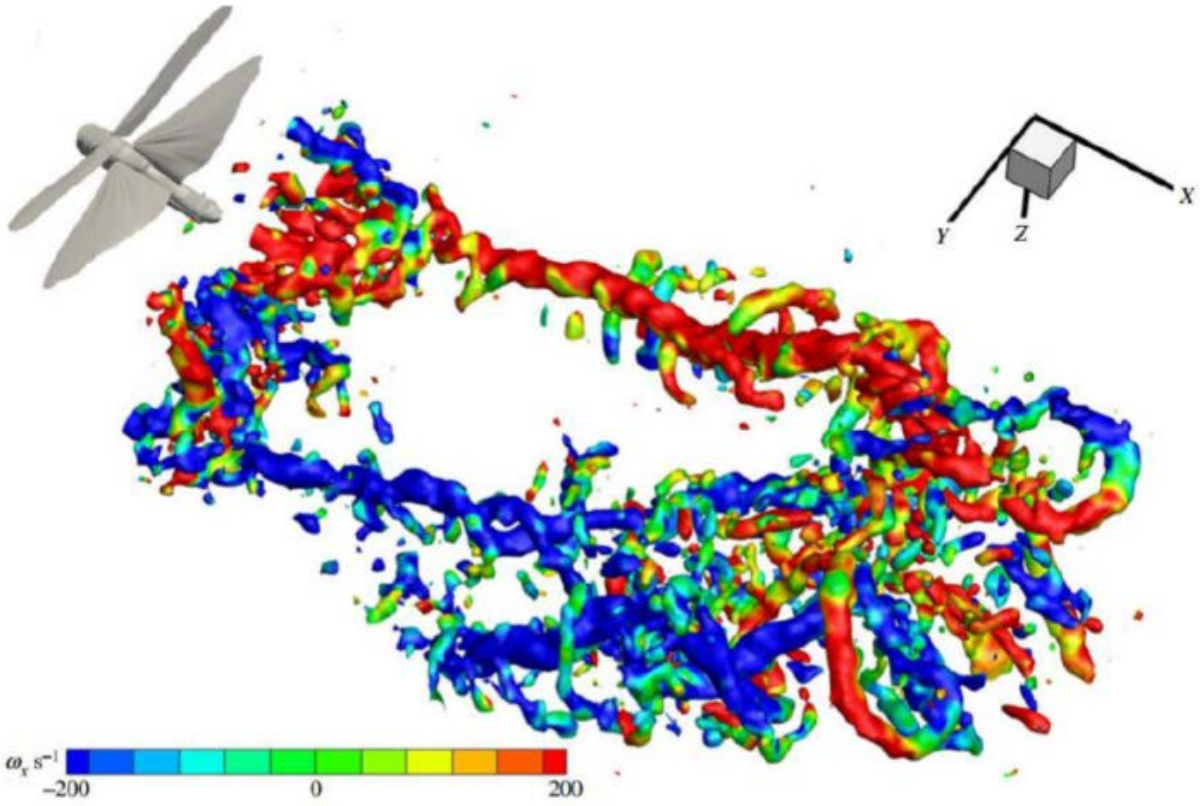

Figure 1. 4 Instantaneous flow measurement of a full wingbeat wavelength on a tethered locust, using tomographic PIV (Henningsson et al 2015).

Recently, a high-speed schlieren photography was adapted to study the flow structures of a free-flying hawkmoth (Liu, Roll, Kooten, & Deng, 2018). It was demonstrated the potential of Schlieren photography to capture the formation and evolution of flow structures. Moreover, unlike previous studies, a secondary hind-wing tip vortex was found and gave a better understanding of the vortex loop formation. Flow visualization was accomplished by applying isopropyl alcohol onto the hawkmoth wings to act as a passive scalar that the Schlieren setup can track. However, the same procedure cannot be used on smaller insects such as houseflies for two reasons. First, the high flapping frequency on small insects vaporizes the isopropyl alcohol very quickly. Second, it is not easy to ensure enough alcohol was applied to all the wing surfaces without adding much weight to the wings. Therefore, to extend the applicability of Schlieren photography to study a broader range of insect species, a different method is required.

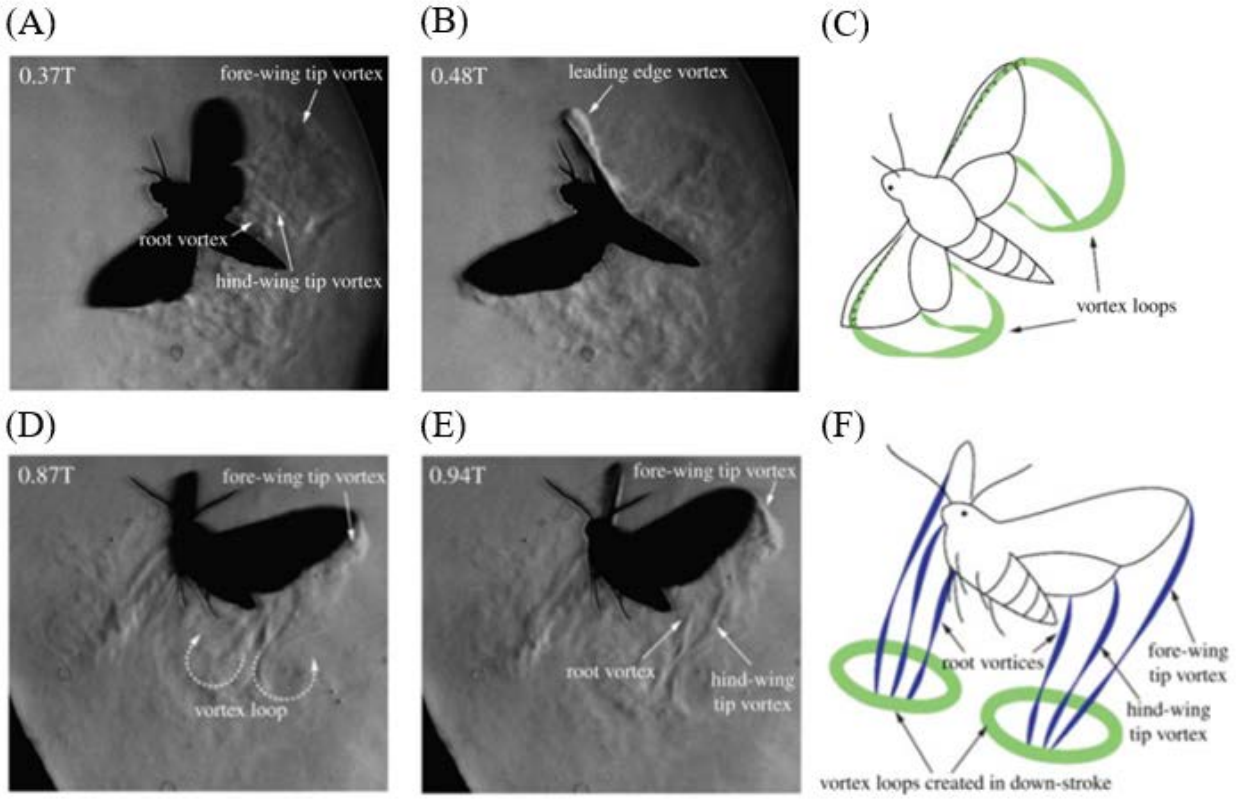

Figure 1. 5 Complete vortex structure captured using Schlieren photography of a hawkmoth (*Manduca*). (Top) Vortex structures during the downstroke. (Bottom) Vortex structures during the upstroke. (Liu, Roll, Kooten, & Deng, 2018)

1.4 Schlieren Photography

Shadowgraph and schlieren photography rely on the index of refraction for flow visualization, which Snell's law can explain. The index of refraction is the ratio of the speed of light in a vacuum to its velocity in a medium. In the presence of spatial variations in the index of refraction, light rays are refracted and deflected from their continuous path. (Taberlet, et al., 2018). Variations on the index of refraction occur if the media's density changes due to local temperature, pressure, or composition (Weinstein, 2010). Schlieren has been used since the early 1800s to visualize and capture fluctuations in optical density (Settles, 2001). The word schlieren (plural, old German) means bits or pieces. It is practiced today based on the techniques first invented by the German physicist August Toepler (Gopal, Klosowiak, Jaeger, Selimkhanov, & Hartmann, 2008). Schlieren is one of the simplest, oldest, and depending on the setup, a cheap method for flow visualization. Schlieren and Shadowgraph photography has been used in fluid

dynamics studies because they are very sensitive methods that do not interfere or disturb flow visualization (Mazumdar, 2013). Another advantage is that the configuration of the Schlieren setup can be easily modified for the needs of different studies. Traldi (Traldi, et al., 2018) published detailed information on different Schlieren setup variations. The basic idea is to use a point light source and direct it to a parabolic mirror, where the light is collimated and travels back to the focal point, where the light is cut off, producing Schlieren images. The cutoff ratio is essential to visualize flow features; typically, 50% of the light is cut. Although the setup of Shadowgraph (0% light cutoff) and Schlieren are quite similar, Schlieren is more sensitive to changes in the index of refraction (Davies, 1981). For a long time, Schlieren and Shadowgraph were used only as a tool for flow visualization or, in some cases, for minimal data extraction, due to the lack of a tool to generate velocity fields.

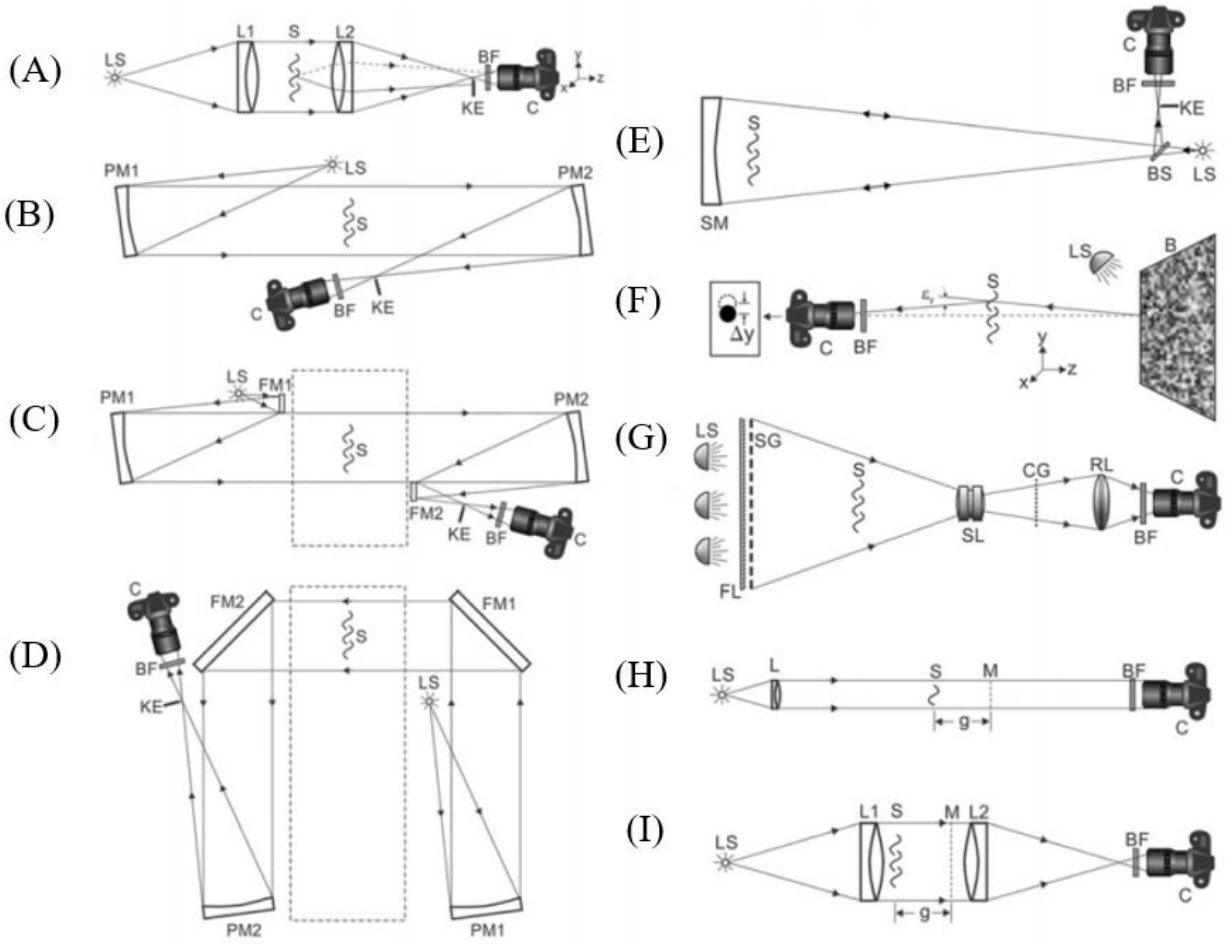

Figure 1. 6 Different Schlieren setup (Traldi, et al., 2018).

1.5 Optical Flow Method

Flow visualization provides a general description of flow behavior, but quantification of flow phenomena is fundamental to comprehend the physics behind the fluid motion. Early attempts to quantify schlieren images can be traced back to 1936 when Townend tracked displacements manually to get velocity measurements. Since this is time-consuming and introducing human errors, schlieren was limited to visualization only for a long time. With the rise of computer technology, particle image velocimetry (PIV) technique has become a widely popular tool to study flow phenomena. PIV is based on the local spatial cross-correlation between two successive particle images to create a vector field (Adrian, 1991). The natural idea was to use the PIV algorithms in schlieren photography; this approach is called schlieren image velocimetry (SIV). However, there are not particles (seeding) to track in schlieren images, leading to poor performance (Hargather, Lawson, & Settles, 2011). To solve this issue, other algorithms based on optical flow rather than particle tracking were developed. Optical flow can be described as the apparent motion of objects in images caused by the relative motion of objects and the viewer (Horn & G.Schunck, 1981). The optical flow equation establishes a link between the spatiotemporal radiance variation from an emitting object in 3D space and its projection onto the image plane (Heitz, Mémin, & Schnörr, 2009). In the optical flow method, the vector field is calculated by assuming intensity constancy between two-time sequenced images (Ray, 2011).

To develop a method to quantify a sequence of images, Horn & Schunck (1981) proposed the brightness constraint equation for computing optical flow. Even though the equation assumes that image intensity does not change during the time sequence. This approach is not derived from any physical principle, and therefore it is not justified from a physical point of view (Liu & Shen, 2008). Moreover, the brightness constrain equation was used for PIV images, and it was concluded that the equation is not accurate to study flow behavior (Ruhnau, Kohlberger, Schnörr, & Nobach, 2005). Another approach was proposed by (Corpetti, Mémin, & Pérez, 2002), who use the continuity equation of fluid mechanics to generate vector fields. Even though this method can generate an accurate velocity field, it is not applicable to every flow phenomena. A general physics base algorithm was proposed by Liu & Shen (2008). They established a quantitative connection between optical flow and fluid flow by deriving a relationship between the radiance projected to a camera and the path-averaged velocity field weighted with a relevant field quantity.

1.6 Aim of the Thesis

Even though flow visualization measurement techniques have progressed considerably, it is still challenging to visualize and measure the complex flow field on small flying insects with current experimental approaches. As mentioned previously, most of the aerodynamics research on small insects was conducted on scaled mechanical models that mimic the flapping wing motion or with CFD simulations. However, it raises concerns on if the mechanical model was able to mimic the details of insect wing morphology; or if the numerical simulation is truthfully reflecting the actual flow of insects. To address this issue, schlieren photography was successfully introduced to study a hawkmoth, but the same method cannot be applied to small insects. In this thesis, a different approach to visualizing flow structures on small insects is introduced. Instead of using isopropyl alcohol, a refraction index gradient was introduced by controlling the temperature gradient in the air. This concept has been successfully implemented by Veldhuis, who used schlieren photography to study the wake structures of rising and falling spheres inside a water tank by creating a temperature gradient (Veldhuis, Biesheuvel, Wijngaarden, & Lohse, 2004). In this study, a small air container is heated on the top and cooled at the bottom to set a refraction index gradient and to capture the flow disturbance generated by houseflies with a Z-type Schlieren setup. To quantify the schlieren images, an optical flow method is implemented to derive velocity fields. This thesis is organized as follows. To test the schlieren setup and optical flow method, in chapter 2, the exhaust gas/ free jet from a matchstick rocket is studied and analyzed. In chapter 3, the new setup of schlieren photography on small insects is described and introduced. The unsteady wake flow is then quantified with optical flow method. In chapter 4, the state-of-the-art “Shake-the-Box” system is implemented on tethered houseflies to resolve the complex 3D flow field in the wake of the tethered insects.

2. UNSTEADY FLOW VISUALIZATION AND QUANTIFICATION OF FREE JET OF MATCH ROCKETS USING SCHLIEREN PHOTOGRAPHY AND OPTICAL FLOW METHOD

2.1 Introduction

Chemical rockets burn fuel in the combustion chambers, converting chemical energy stored in the propellant into high pressure/kinetic energy to push exhaust gas through the nozzles, producing thrust. One simplest example of chemical rocket is matchstick rocket that can be easily built with matchstick and aluminum foil. Aluminum foil wraps around a match head, which is essentially a mixture of solid fuel and oxidizer and can be heated up from the outside to initiate the combustion inside the small chamber of aluminum foil. The modern matches are usually made of mixture of potassium chlorate, sulfur, and phosphorus (Mohamed, Sivapirakasam, & Surianarayanan, 2013). When heated, the propellant burns and creates predominantly hot, low-molecular-weight gases in the confined space to produce a high pressure that push the gaseous product out of the chamber from a small opening at the tail. Although the matchstick rocket has many design variations and appeared in several educational books as an experimental experience to understand Newton's laws (Gurstelle, 2012; Nations, 1988), there is very little scientific study on the exhaust gas flow of matchstick rockets.

Meanwhile, the exhaust gas flow from the rocket can be characterized as a free jet which is directly discharged into the ambient air. A free jet can be described as the interaction of a fluid with some momentum or buoyancy exiting from a narrow exit into a large static fluid body. The velocity difference between the free jet and static fluid body produces a discontinuity that becomes unstable and generates vortices that entrainment the surrounding fluid into the jet (Chang, et al., 2020). Those vortices, fuse, pare, and rupture during the development of the jet, and play an important role in the characteristics of the jet. Based on the velocity center line decay, the jet flow can be divided into four different velocity zones: core, transition, profile similarity, and termination (Kmecova, Sikula, & Krajcik, 2019). Free jets have been studied experimentally with different methods, including dye visualization, hot wire measurement, particle image velocimetry, and schlieren photography. Schlieren photography can be implemented because normally, the densities between the free jet and static fluid body is

different, which can be perceived by the method. In this study, a high-speed schlieren photography is implemented on free jets produced from two horizontally anchored match rockets, one with skewer stopper at exits and another without it. To quantify the velocity field of the free jet, a physics-based optical flow method (Liu & Shen, 2008) is implemented on the schlieren images.

2.2 Materials and Methods

Our match rockets are made of aluminum foil, bamboo skewer, and match head. The aluminum foil was cut into a trapezoidal shape (30 mm x 115 mm). A 20 mm long skewer and match head were put along the longer side of the aluminum foil, covering 20 mm aluminum foil and leaving 10 mm empty. Then, the skewer and match head were wrapped from rolling the aluminum foil to create the cylindrical body of the match rocket. And the spare foil above the match head was twisted and crimped with a pair of pliers. The final length of the rocket was about 30 mm with an exit diameter of 3 mm. Mainly because the skewer inside the rocket is being used as a compression mechanism to increase pressure inside the chamber. Eventually, the matchstick will be pushed out of the rocket due to the exhaust gas. Limiting the rocket exit dimension to the skewer diameter of 3 millimeters. For the second rocket, the same procedure was implemented but with the bamboo skewer removed from the chamber afterward. Once the rocket was complete, it was anchored horizontally on the table and ignited to launch it by heating the rocket head with a lighter under the rocket head.

To capture and visualize the exhaust gas produced by the rocket match, a high-speed schlieren photography system was implemented. The system consisted of a high-speed camera (Photron Mini UX 100), two 10-inch parabolic mirrors, and a LED. The white LED light was projected throughout a 1 mm pinhole into the first mirror, which collimates the light and reflects it to the second mirror, producing parallel rays of light in the test region. The second mirror focuses the collimated light towards the camera, passing by a razor blade edge. The high-speed camera then recorded the schlieren images at 10,000 frames per second at a resolution of 1280x480 pixels. In this paper, two experiments were presented; a match rocket with a skewer in the chamber and one rocket that does not. To derive the velocity vector field, the resulting schlieren images were later processed with a physics-based optical flow method (Liu & Shen,

2008). Due to the unsteadiness of the flow, not only velocity fields were calculated but also acceleration and shear fields were derivative from the optical flow method. Demonstrating, the full potential of this method as a tool to study flow behavior.

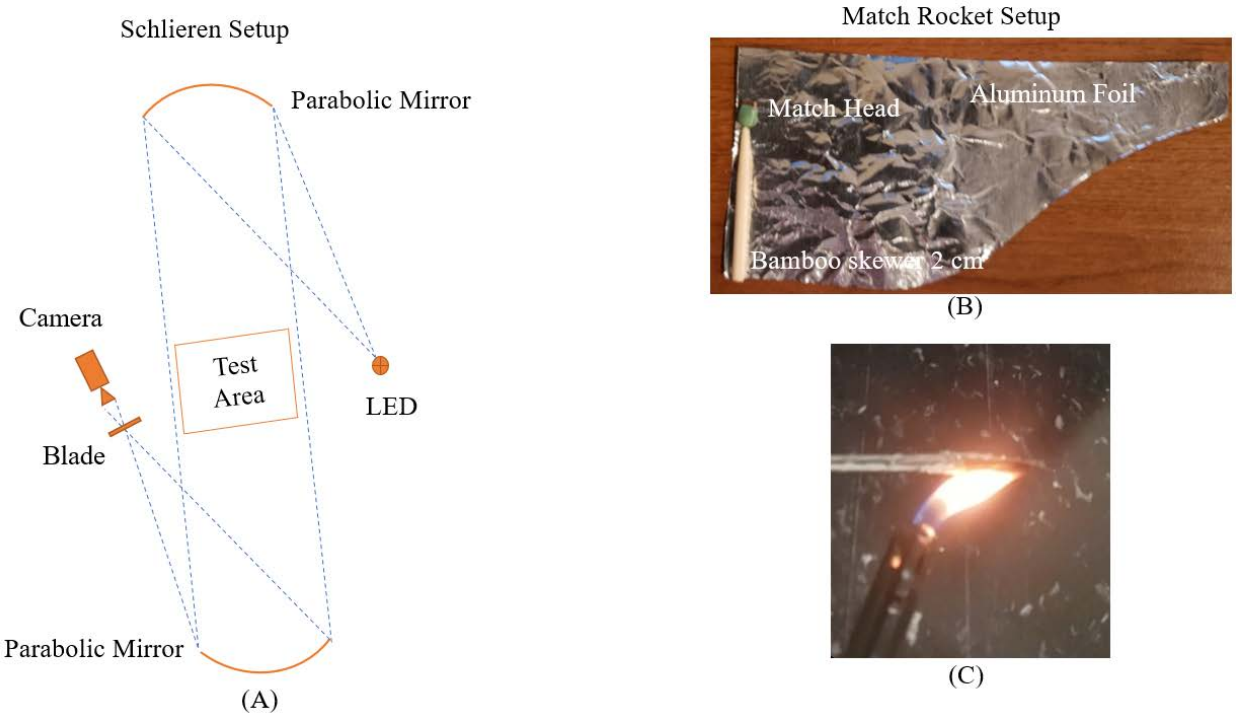

Figure 2. 1 (A) Z-type Schlieren set-sup. (B) Materials used to build a match rocket. Rocket before wrapping the aluminum foil. (C) Rocket after wrapping and ignition.

2. 3 Results

In a rocket engine (liquid or solid), fuel and oxidizer are mixed and exploded in a combustion chamber (Benson, Combustion, 2014), producing new chemical substances (exhaust gas) with high pressure that passed through a nozzle to produce thrust (Hall, 2015). The same principles apply to the match rocket. The match head contains the solid fuel and oxidizer, while the rolled-up aluminum foil acts as the combustion chamber. When the match head burns in the rolled-up aluminum foil chamber, the gasses product expands quickly in the chamber and builds up the pressure, pushing the rocket to move forward. Meanwhile, owing to the reacting force, the exhaust gas will be pushed backward and exits the rocket chamber. When the rocket is tested with a skewer inside the chamber, the chamber is enclosed; thus, the pressure can be built up quickly until it reaches a critical value that can push the skewer out of the chamber. When the

rocket is tested without a skewer, the chamber is open in the end, and exhaust gas flow will be created at the very beginning of the ignition.

2.3.1 Velocity field quantification

With the high-speed schlieren photography system, the exhaust gas with a different density to the ambient can be visualized and captured. The schlieren images are first pre-processed with background subtraction and then processed utilizing the physics-based optical flow method in MATLAB to derive the velocity vector field. The velocity is calculated in a rectangular region (27 mm × 20 mm in physical space and 236×175 pixels in images) at the rocket exit. Figure. 2 *a*, *c* present two samples of the background-subtracted schlieren images of the exhaust gas tested with a skewer and without a skewer. Figure. 2 *b*, *d* present the averaged velocity contour plots (over 30 frames or 3 milliseconds) at time instants when the exhaust gas reaches the highest speed at t = 1.5 ms for a rocket with skewer and t = 40 ms for rocket without the skewer. In the horizontal direction, when the exhaust gas exits the rocket, the gas first accelerates and then reaches the local maximum velocity at a distance of about x = 4.5D (at a distance of five times the rocket diameter), then the exhaust gas starts decelerating in the down-stream. In the schlieren photography images on the match rocket without a skewer, we observed significant dark regions in the exhaust gas flow that could be related to the inadequate combustion product under low temperature and pressure (This phenomenon is repeating on the rockets without skewer). Particularly, in the later part of the schlieren photography video, the dark imaging issue is getting worse and prevents us from applying the physics-based optical flow method to quantify the flow field. Consequently, in the match rocket test without a skewer, only the first 45 milliseconds of the event is analyzed and studied, while an event of 80 milliseconds is analyzed and studied on the match rocket test with a skewer.

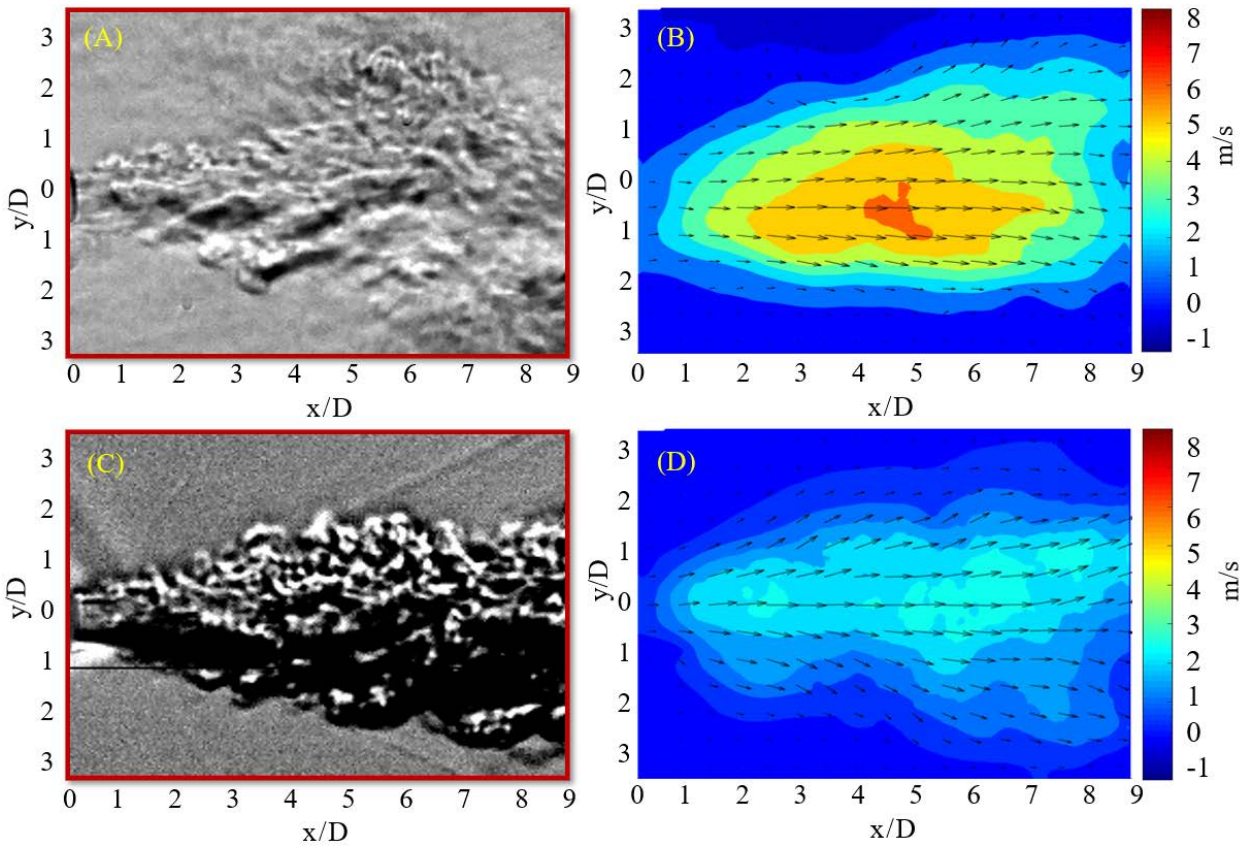

Figure 2. 2 (A & C) Images after background subtraction and boundary region highlighted in color red. (B & D) Vector and contour velocity fields at the highest maximum velocity. (A & B) Match rocket with bamboo skewer at t = 1 ms. (C & D). Match rocket without bamboo skewer at t = 45 ms.

Only the axial component of the velocities was considered because the thrust is only correlated to the momentum in the axial direction. Fig. 3 *a*, *b* shows the velocity plots on the rocket with a skewer and Fig. 3 *c*, *d* show the velocity plots on the rocket without a skewer. In Fig. 3 *a*, *b*, the raw instantaneous local maximum, and spatial average velocity, plotted in blue, fluctuate substantially. A moving average filter with a window size of 3 milliseconds is applied to the raw data, deducing filtered data in red. The filtered result shows that the local maximum and spatial average velocities are at the highest in the beginning with a value of 9.99 m/s and 2.37 m/s, respectively. Both the local maximum and spatial average velocities are continually decreasing over time. On the rocket with the skewer, because the solid propellant is limited and combustion happened in a very short time of duration within the confined space, the chamber/total pressure is highest when the exhaust gas pushes the skewer out of the chamber. Therefore, the flow momentum is at the highest value at the beginning of the event. On the rocket without the skewer, however, the local maximum and spatial average velocities are at the

lowest values in the beginning of the event and continually increasing over time. During the time of investigation (the velocity quantification is limited to the first 45 millisecond due to the dark images), the filtered local maximum and spatial average velocities reach to the highest value of 7.73 m/s and 1.16 m/s, respectively at the end of the time. On the rocket without the skewer, since the chamber is not enclosed and with an open end, the exhaust gas flow is created immediately after the combustion started. Due to the non-uniform heating on the solid propellant, the combustion is localized in the beginning and then starts in other places to eventually reach a complete ignition (Was observed in testing on the match head). Therefore, without an enclosed chamber, in Fig. 3 *c* and *d*, before reaching the highest value, the chamber/total pressure is increasing over time, so as the exhaust gas speed.

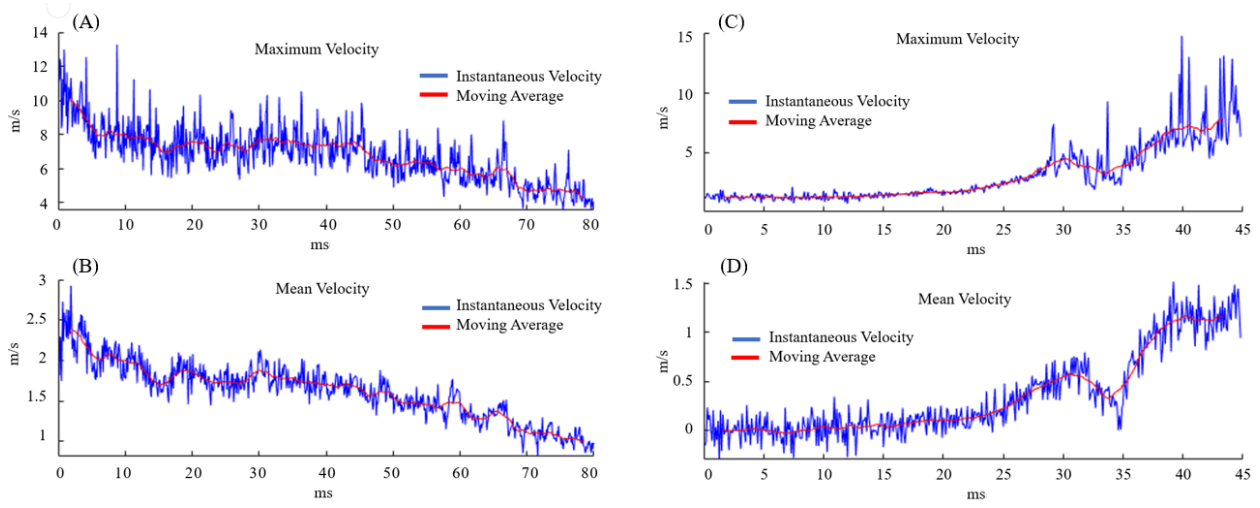

Figure 2. 3 Instantaneous and filtered maximum and mean velocities of both rockets. (A & B) Match rocket with a bamboo skewer. (C & D) Match rocket without a bamboo skewer.

Comparing the exhaust gas speeds between the two match rockets, the exhaust gas speed is higher in the rocket with the skewer but lower without the skewer. Assuming the solid propellant are similar between the two rockets, during the combustion, the chamber/total pressure in a confined space should be higher than the one in an open chamber, resulting in a higher momentum in the exhaust gas flow. Moreover, when the exhaust gas of the two rockets reaches the highest speed, the instantaneous velocity profiles are examined at three different distances from the rocket exits and presented in Figure 4. Similar to the observation in Figure 2, on both rockets, the exhaust gas accelerates at the beginning from the exit and reaches to the

highest spatial velocity at a distance of 4.5D from the exit. Comparing the velocity profiles from the two rockets, the velocity profiles at the exits (x=0) have a similar velocity magnitude of about 2 m/s. However, at x = 4.5D the exhaust gas velocity is considerably higher on the match rocket with the skewer at a speed of 6 m/s at the center and lower on the rocket without the skewer at a speed of 4m/s at the center, which further substantiates the observation in Figure 3. In addition, the jet of the rocket with the bamboo skewer does not have a perfect conical shape due to the exhaust gas at the beginning is constantly hitting the back of the expelled skewer. Eventually, the disturbed flow is dissipated and recovers its traditional conical shape.

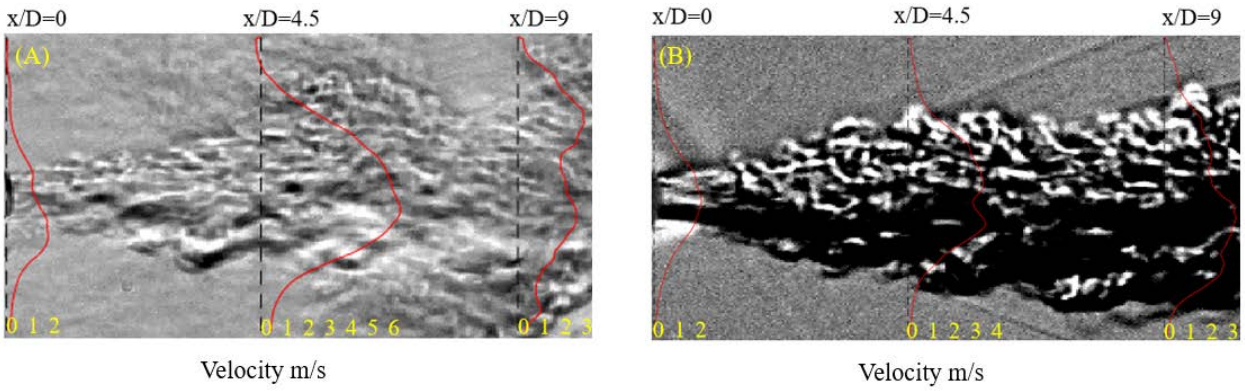

Figure 2. 4 Velocity profile at the instant of maximum velocity at three different locations. (A) Match rocket with a bamboo skewer at t = 1 ms. (B) Match rocket without bamboo skewer at t = 45 ms.

On the other hand, mean acceleration (material derivative), mean velocity, and mean shear were calculated on the rocket with the skewer to investigate the detailed physical process of the exhaust gas flow. The rocket without the skewer, however, developed a vortex ring in the beginning before producing the jet flow. This happened because low energy jet intends to create a vortex ring at low Reynolds numbers (Chang, et al., 2020). Afterward, as the pressure in the chamber increases, and the jet Reynolds number increased and developed into standard conical shape free jet flow. Therefore, the flow field changes substantially on the rocket without the skewer and is not considered in later calculations. The rocket with the skewer showed an interesting phenomenon of acceleration-deceleration-acceleration (Figure 5 a). Where it can be seen that at the exit, there is a high acceleration followed by deceleration. However, there is a transition zone where the exhaust gas accelerates once again to finally decelerate at x= 7.6 D. Therefore, two velocity peaks are observed along the centerline of the flow, with the first peak at

3.5 m/s and a second peak at 3 m/s. Moreover, it is expected that local pressure at the second mean velocity peak (x= 7.6 D) should be equivalent to ambient pressure where the flow in downstream is purely driven by inertia and decelerate under friction.

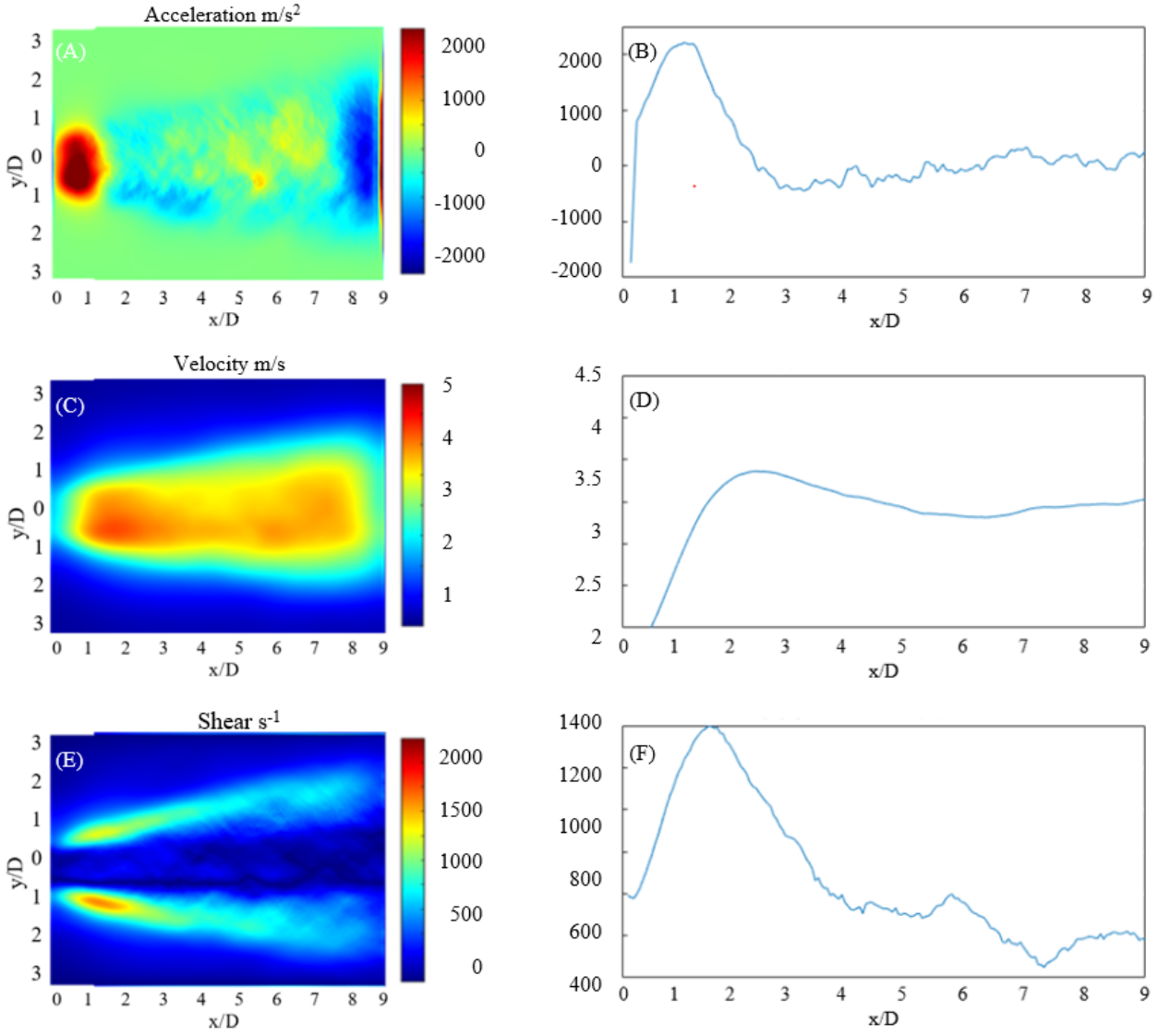

Figure 2. 5 (A, C, E) Time average over 80 ms of acceleration, velocity, and shear field, respectively. (B) Acceleration along the centerline. (D) Mean along the centerline. (F) Mean shear along the bottom layer at y/D =1

Also, the mean acceleration, mean velocity, and mean shear at the exit are not symmetric. This issue persisted on different trials where there was a small leak either at the top or bottom. For two reasons, the exit is not symmetric because the aluminum foil was not well wrapped, or

the pressure inside the chamber is too high that breaks the weakest zone at the exit. This also concatenates on higher shear stress at the exit bottom than the top shown in Figure 2.5 e, f. In addition, the bottom shear layer is ticker and extends for a longer distance than the top layer. Indicating that the discontinuities due to the velocity difference between the exhaust gas and the surrounding air are more prominent in the bottom than in the top. Also, the top and bottom layer of the jet has different mixing rates between the air and the exhaust gas, since this is dictated by the shear layer (Chang, et al., 2020). Moreover, in Figure 2.5, e there is a significant and continuous drop of shear stress magnitude along the bottom section of the jet.

2.3.2 Thrust force estimation

As the instantaneous velocity field is obtained, the thrust force can be estimated by implement the conservation of linear momentum. To estimate the thrust some assumptions were made. (1) The exhaust gas can be treated as ideal gas. (2) Chemical equilibrium is established within the rocket chamber, and the gas composition does not change over time. (3) The rocket exit is axial symmetric. Applying these assumptions and conservation of the linear momentum (Sforzini, 1970), the thrust is estimated with Equation 1 and Equation 2.

$$F = \frac{\partial}{\partial t}\int_{CV} v(x,t)\rho dV + \int_{CS} v(x,t)\rho v(x,t)dA \quad (1)$$

$$F = \frac{\partial}{\partial t}\int_{CV} v(x,t)\rho dV + V_{x1,mean}^2 \pi {r_1}^2 \rho + V_{x2,mean}^2 \pi {r_2}^2 \rho \quad (2)$$

$$16\ KClO_3 + 3\ P_4S_3 \rightarrow 6\ P_2O_5 + 16\ KCl + 9\ SO_2$$

The first term in Eq.1 is the rate of change of fluid momentum inside the control volume. While the second term is the momentum flux going out of the control volume (Dabiri, 2005). Since the exit rocket is not symmetric, velocity along r_i will vary. To address this issue, two approaches to estimate the velocity were considered. In the first approach, velocity for each r_i was calculated by taking the mean value of each r_i for Eq 1. In the second approach, the overall

mean velocity at each control surface was used on Eq. 2. In the case of ρ density, ideal gas law was used for SO_2 as it is the primary gas product from the chemical reaction. A thermal camera (Flir E40) was used to measure the temperature of the exhaust gas, deriving a temperature of 96 ^{o} C, therefore a gas density of 2.1175 kg/m^3 is derived. Equations 1 and 2 are implemented on a control volume, the black rectangular boundary in Figure 2.6, in which the green line sits at the exist of the rocket and green line 2 lays at the second velocity peak, and local pressure equals to the ambient pressure.

The estimated thrust (pressure at exits) increases until it reaches a maximum value around t=10 ms. Eq. 1 has a maximum thrust of 0.012207 N at 10.9 ms, while Eq. 2 has a maximum value of 0.012556 N at 9.3 ms. This follows a common curve of a rocket thrust graph. However, after this peak usually there is a drop in thrust followed by a steady/constant zone. In the case of the matchstick rocket is not the case, and instead, thrust drops continually in the process. This can be attributed to the uneven combustion of the head match. Since the combustion ratio of the fuel and oxidizer is not precisely controlled, the kinetic energy released changes over time and therefore changes the rocket's thrust. On the other hand, comparing the two-equation, there is an overall discrepancy of 0.000256 N between them. Also, it can be seen that Eq. 2, in general, has higher values than Eq. 1.

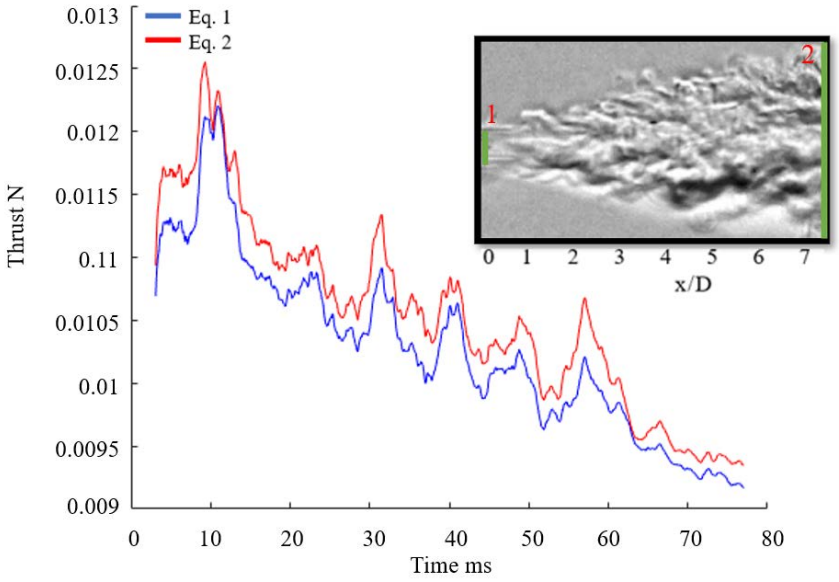

Figure 2. 6 Plot of thrust using Equations 1 and 2. Control volume highlighted in black and controls surfaces highlighted in green.

2.4 Discussion

Studying the exhaust gas flow produced from a match rocket is complex. The exhaust gas flow is unsteady, and the rocket exit is not symmetric. In addition, replicate the same procedure for each rocket is challenging. Match head size, effectiveness wrapping the bamboo skewer, and other variables make the match rocket performance vary from to trial to trial. In addition, even though the match head can be considered a solid propellant, the design differs from a standard solid propellant with a cylindrical shape. Usually, with a perforation in the center along the cylinder to control the chemical reaction of the elements and direct the exhaust gas to the exit/nozzle. This means that the match head does not have an optimal design for a solid propellant. Causing the chemical reaction/combustion of the fuel and oxidizer not being well controlled and producing fluctuations in pressure and exhaust gas expelled. Also, unburned and burned material exiting the rockets contributes to the uncertainty of the velocity quantification. Moreover, considerable velocity fluctuation is observed in the velocity quantification, which can contribute to the solid propellant's imperfection. Despite of these, both graphs follow a similar trend, providing an insightful description of the exhaust gas behavior.

Some modifications of the setup can help for future studies. Only wrapping the head match and using a small diameter pipe for the rocket body could solve the issue of the exit geometry. Also, smashing the match head to make powder from it and weigh it for each trial can standardize the procedure to understand the fluid flow better. Other brands might use different ratios of chemical elements to make the head match. Also, to increase the performance of the rocket, a nozzle must be used instead. This can be accomplished by replacing the bamboo skewer with a small valve. Since the purpose of the skewer is to keep the gas inside the chamber to increase the pressure. A closed valve can do the same, and by opening the valve, the gas can be redirected through a nozzle. On the other hand, the optical flow method appear to be an excellent tool to study flow phenomena comminated with Schlieren photography.

3. ADAPTING SCHLIEREN PHOTOGRAPHY TO VISUALIZE FLOW STRUCTURES OF A TETHERED AND FREE FLYING HOUSEFLY

3.1 Introduction

Insects perform flapping-wing flight to create lift and thrust for forwarding and backward flight while achieving remarkable maneuvers with rapid accelerations and decelerations (Liu H., 2009). For example, a fly can change direction by 90° in less than 50 milliseconds while flying through the air (Fry, Sayaman, & Dickinson, 2003). Insect flight has fascinated researchers because applying fixed-wing aerodynamic theories to study their flight led to the contradiction that insects should not fly. The small wing size and high angle of attack flight do not satisfy traditional aircraft theories. This promoted the rapid growth of experimental research in the past decades to study the complex flow structures generated by insect flight to understand their aerodynamic mechanisms. For example, using smoke visualization on a tethered hawkmoth, the leading-edge vortex (LEV) was captured and linked as the primary source of lift production, solving the enigma of how insects are capable of flying. (Ellington, Berg, Willmott, & Thomas, 1996). Nowadays, it is believed that the LEV can generate up to two-thirds of the total lift in insect flight (Muijres, et al., 2008). Similarly, many studies have found other mechanisms such as: added mass, rotational circulation, clap and fling, and wing–wake interaction, that insects utilize to generate aerodynamic forces (Chin & Lentink, 2016). Also, there has been a lot of work on deriving theoretical expressions of force estimations based on properties of vortex wake (Dabiri, 2005) because the vortex wake can be considered the “footprint” of a traveling insect (Wang, 2005).

Particle image velocimetry (PIV) has been used to qualitative and quantitative study the unsteady flow of large insects revealing complex vortex structures. However, most of the studies of small insects have been performed using mechanical flappers, because conventional particle-tracking flow measurement methods cannot efficiently resolve the flow structure even with high-density seeding. Advancement in technology and particle tracking algorithms made it possible to capture three-dimensional vortex structures on a tethered locust using tomographic PIV (2015) (Henningsson, et al., 2015). However, it was limited only to the far-field wake, leaving uncertainties in the flow structures near to the wings. Moreover, it took 96 days to reconstruct the

flow structures on sever server with 48 AMD cores and 64 GB of ram. In addition, the setup consisted of a powerful laser and eight cameras (high-resolution and high-sensitive). Making this set-up very expensive and not realistically possible to replicate in other laboratories around the world.

Most of the studies of insect aerodynamics were made on large insects such as: dragonflies, locusts, and hawkmoths, bumblebees, droneflies, and hoverflies (Cheng & Sun, 2016) because it is difficult to study a small insect in a natural setting. Therefore, there is not too much research on real small insects. Advancements in computational power made it possible to simulate insect flight. In addition, technology help to design detailed robotic flappers to study small insects. To develop a model, some critical parameters such as: angle of attack, stroke amplitude, and wingbeat frequency are usually acquired using high-speed cameras. This data is used as input for the CFD simulation or to design mechanical flappers. Using this data, both models provide a complete visualization of the formation and evolution of the vortical flow. However, insect wings still are very complex to model because of their deformable structure and unique features that might be easily overlooked. Therefore, these two approaches raise the concern if the model was designed considering all the details of insect wing morphology and whether the mechanical and numerical simulation is truthfully reflecting the actual flow generated by an insect. Consequently, despite that many studies have significantly contributed to decipher the aerodynamic mechanisms of the flapping flight, there is not a fully comprehensive understanding of the complex flow structures and the aerodynamics of hovering insects. One of the reasons is that it has been challenging to observe the complete flow structures in the near-field and far-field wake on real insects.

Schlieren photography has been used in fluid dynamics studies because it is a very sensitive method that does not interfere with or disturb flow visualization (Mazumdar, 2013). As with any other method to study flow phenomena, this technique has improved with advancements in technology. High-speed cameras and optical flow algorithms made it possible to use it as a qualitative and quantitative method for a broader range of applications. This non-conventional method to study flying insects was recently adopted to investigate a free-flying hawkmoth (Liu, Roll, Kooten, & Deng, 2018). Demonstrating the potential of this method to fully capture the formation and evolution of the vortical flow structures. The flow was captured by brushing isopropyl alcohol onto the wings to act as a passive scalar to be tracked by the

Schlieren setup. However, this method cannot be used on smaller insects such as house flies because of two reasons. First, the high flapping frequency vaporizes the isopropyl alcohol very quickly. Second, it is difficult to ensure enough alcohol was applied to all the wing surfaces without adding too much weight to the wings. Therefore, to extend the applicability of Schlieren photography to study a broader range of insect species, another method was needed. Veldhuis used Schlieren photography to study the wake structures of rising and falling spheres by creating a temperature gradient inside a water tank (Veldhuis, Biesheuvel, Wijngaarden, & Lohse, 2004). This paper implements a similar approach to study a tethered house fly inside a container filled with air heated on the top and cooled on the bottom to develop a temperature gradient to capture the disturbed flow filed with the Schlieren setup.

3.2 Materials and Methods

Experiments on house flies were performed on the third day after they hatched. A housefly was tethered following the procedure suggested by Duistermars. A housefly was placed inside a refrigerator at 4 ^{o}C for anesthetizing the insect. Then, a small pin with a diameter of 0.072 inches was glued to the dorsal thorax between the head and the two wings. Finally, the fly was left to recover for about 10 minutes before inserting it inside the testing container. A small container (80 x 40 x 50 mm) was build using optical glass, transparent acrylic sheet, copper plate, and aluminum water block. The optical glass was used for the front and back walls, while the acrylic sheet was used for the side walls. An easy openable/closable window was made on one of the sides for putting the insect inside the container when the temperature gradient was stable. The temperature gradient inside the container was built by heating the top at 40 ^{o}C (copper plate) and cooling the bottom at 0 ^{o}C (aluminum water block). Two ptc electric heaters were glue to the copper plate to heat it, and a PID controller was used to keep the temperature at a constant value. To cool the aluminum block, a liquid cooling loop system was implemented that consisted of a pump, refrigerator, and windshield liquid. The windshield liquid was cooled before it was pumped to flow in the loop. A PID controlled was also used on the bottom to keep a constant temperature of 0 ^{o}C. In reality, it was difficult to control the temperature on the top, and the bottom at there was a discrepancy of ± 4 ^{o}C.

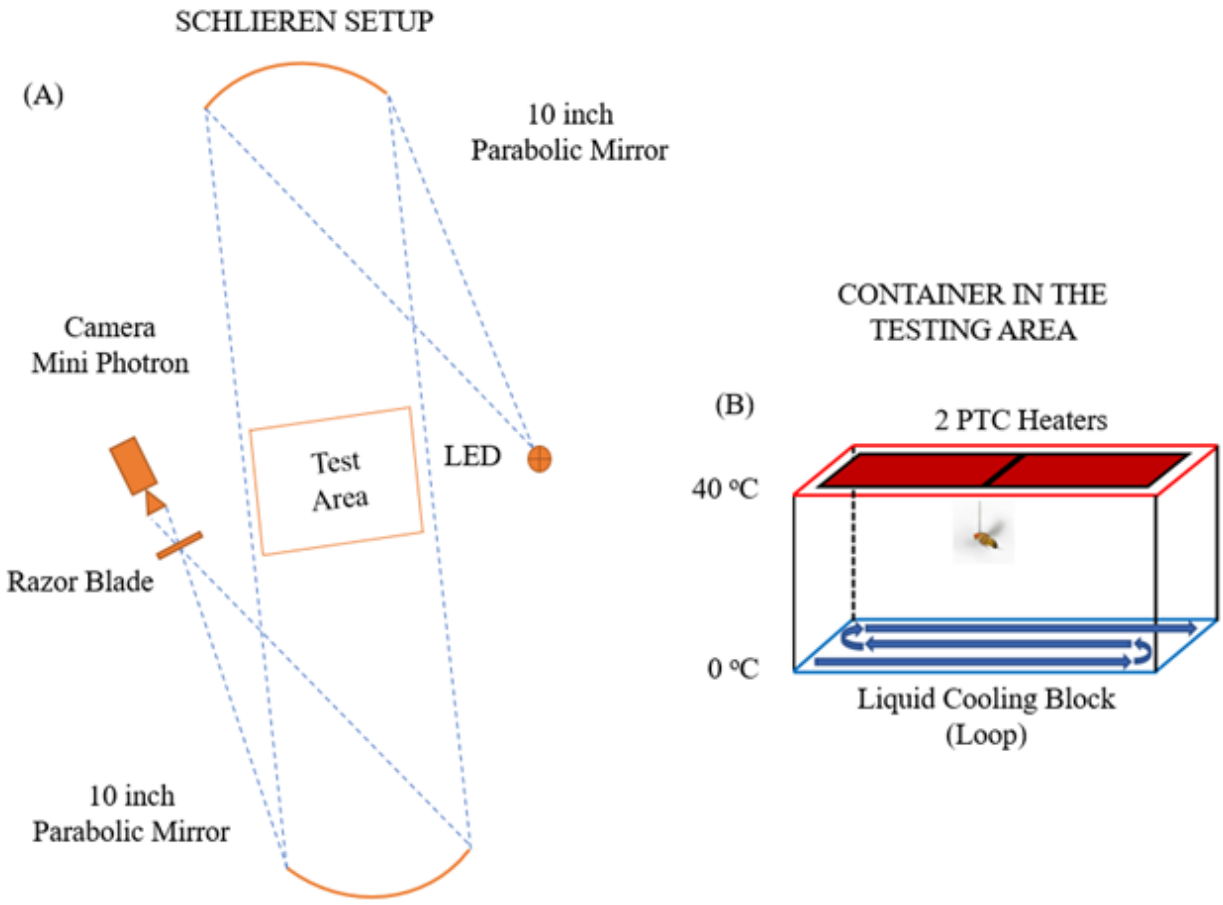

Figure 3. 1 (A) Z-type Schlieren setup. (B) Setup and temperature of the container (80 x 40 x 50 mm) in the testing area. The top of the container was heated with two thermal electrical heaters, and the temperature was controlled with a PID controller. The bottom is cooled using windshield liquid as a coolant in a loop. The liquid at low temperature leaves from the refrigerator and goes through the cooling block, and returns to the fridge to repeat the cycle.

A standard Z-type high-speed Schlieren photography system was used to capture the flow field with a high-speed camera (FASTCAM Mini UX 100). Two 10-inch diameter parabolic mirror were used to collimate and refocus the light source from a white LED. In the case of the tethered housefly, a 300 mm lens was used. On the other hand, A Nikon 500 mm zoom lens was used for the free-flying housefly. A Schlieren video was captured at 10,000 frames with a resolution of 1280 x 480 pixels. The images were pre-processed using background subtraction to delate minor imperfections of the optical glass. Then a physics-based optical method (Liu & Shen, 2008) run on MATLAB was used to quantify the disturbed flow produced by the housefly.

Since Schlieren photography depends on the refractive index to visualize flow phenomena, which directly correlates with the temperature gradient, the container's temperature

was studied. It was used a thermal camera (Flir E40) to record the container's temperature for 25 minutes. Although, the temperature gradient in Figure 3.3 does not represent the actual temperature inside the container because the camera is recording the optical glass temperature. This graph allows to demonstrates that a temperature gradient is successfully implemented, and also to visualize the temperature distribution. In addition, it will enable to test of the performance of the heating and cooling device. Moreover, this help to have an idea where to place the insect in such a way to not harm the insect due to the high temperature, while ensuring high contrast on the Schlieren video. The recorded video data was extracted using the software FLIR Tools + and plotted using MATLAB (Figure 3.3). Only the first 13 minutes were plotted because from that minute, the heaters on the container's top keep a constant temperature of 90 ^{o}C. In addition, at that instant, it can be seen an almost perfect linear relationship. Implying, the temperature gradient is evenly distributed from top to bottom. Also, it was found that after 20 minutes, the cooling device lost its efficiency and started to raise the temperature to almost 20 ^{o}C. However, this is not an issue since the videos are recorded within the first 10 minutes.

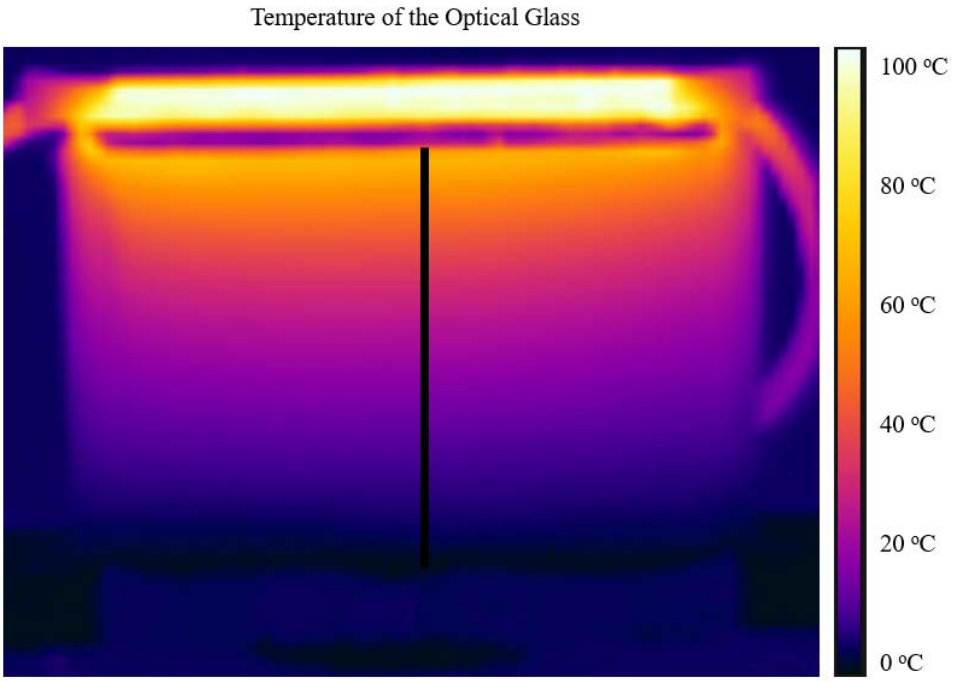

Figure 3. 2 Temperature distribution of the glass container recorded with a thermal camera (Flir E40). The temperature along the black line in the middle of the container is measured using FLIR Tools +.

The temperatures plotted in Figure 3.3 are along the black line in Figure 3.2. Although in figure 3.4 the temperature reaches 90 ^{o}C, that only happens after waiting for 13 minutes. In reality, the experiment is performed at t=2 min and the temperature inside the container at the top is 40 ^{o}C at the very top (measured with a thermocouple). This is corroborated in figure 3.3 where it can be seen that the heated copper plate is colder than the optical glass. In addition, the temperature where the insect is placed was around 35 C, and the fly was perfectly able to fly, including untethered flies. The temperature in the glass can be due to the thickness of the optical glass and the direct contact of the copper plate and optical glass. Unfortunately, no thermal properties of the optical glass were available to have a better understating of the heat exchange and correlated it with the air inside the container.

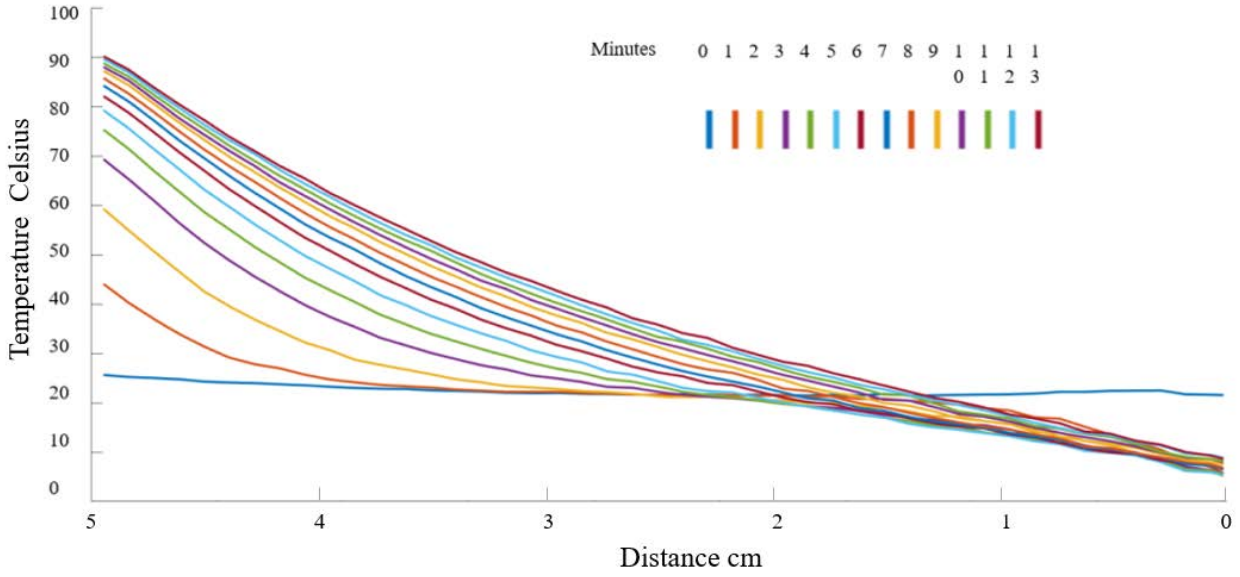

Figure 3. 3 Vertical temperature distribution of the optical glass taken at the middle of the container for 13 minutes. The vertical distance is measured from the top to the bottom of the container.

3.3 Results

In figure 3.4 is presented the steps implemented to visualize and quantify the flow structures of a tethered housefly. Once the Schlieren video is recorded, the images are pre-proceed using a background subtraction code run in MATLAB. This step is for subtracting the static objects and slight imperfections in the optical glass, lens, and parabolic mirrors. In addition, this enhances the flow signal that is hard to visualize on the raw images. In total, fifty

images were used to generate the background that will be used to subtract for each image. The white spots around the housefly are due to this step, but it will not affect the flow quantification. Then, the vector velocity field of the enhanced image is obtained by running a code in MATLAB based on a physics optical flow method (Liu & Shen, 2008). The boundary highlighted in blue in figure 3.4,b will be used in this chapter to estimate the velocity field. Even though in figure 3.4,c there places where there should not be vectors calculated, the overall estimation in those places is close to zero, as can be seen in figure 3.7,b,d.

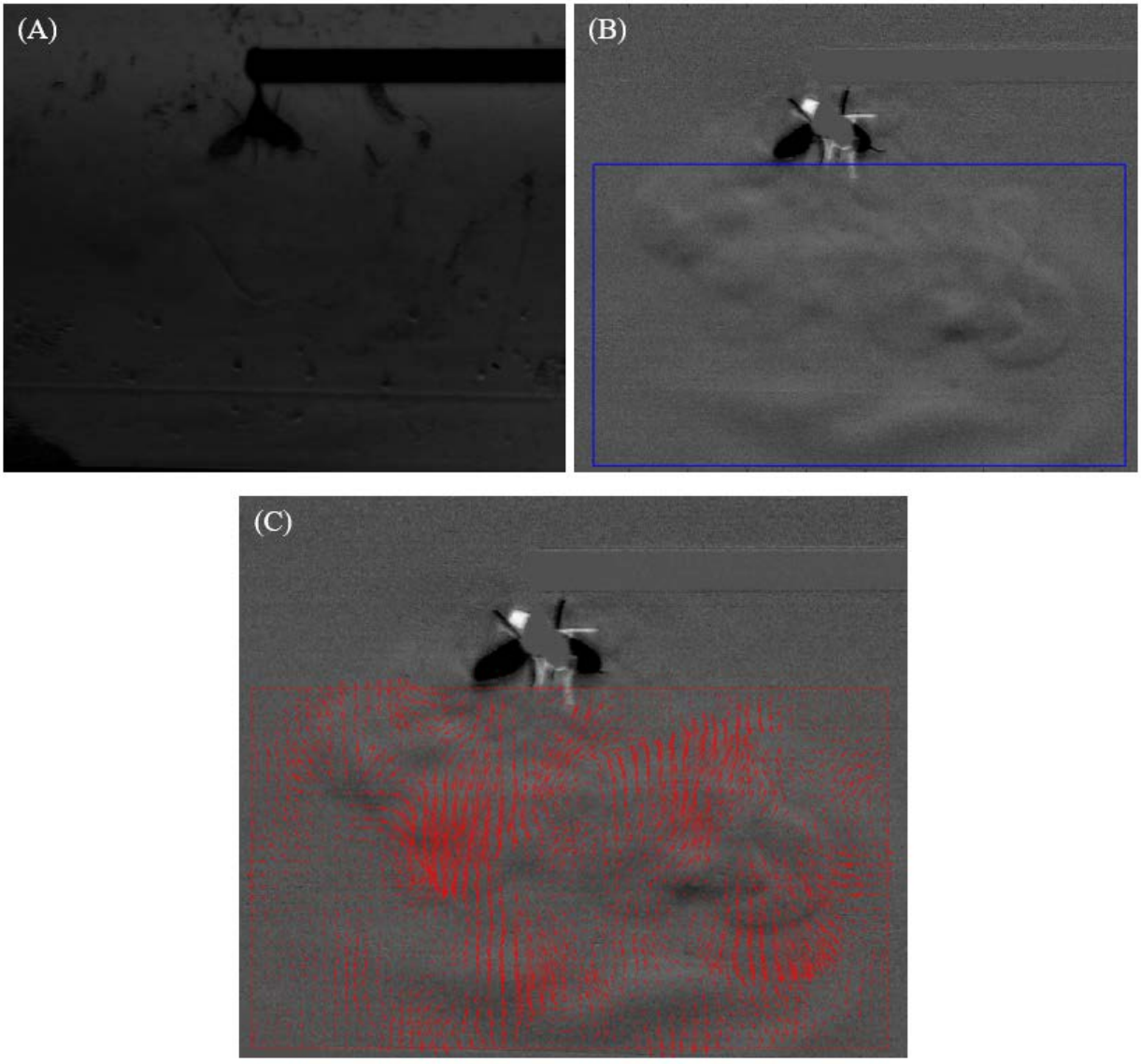

Figure 3.4 Procedure to quantify Schlieren images. (A) Raw image. (B) The image is pre-processed using background subtraction to enhance the signal and delate small imperfections in the glass. (C) Vector velocity field using optical flow method (Liu & Shen, 2008).

As it can be seen in Figure 3.4 b, the entire disturbed flow field by the housefly is very clear to see. Demonstrating that the vertical temperature gradient approach can be used to study small insects. However, some limitations and improvements still exist for this approach to capture all the flow structures. First, after processing the video, there was a considerable amount of noise in the images, most likely caused by the high frame rate and illumination. This was addressed by applying a denoise and illumination filter to the pictures before running the optical flow code. Second, the video was recorded with a 300 mm zoom lens that is clearly not enough to have a closer look at the insect body. Therefore, the resolution is not high enough to distinguish some vortices and carry out an analysis closer to the wings. The setup was also tested with a 500 mm zoom lens, but the images got darker, which increased the noise, even at a lower frame rate. This was because the light was cut off with the razor blade at the focal point and by the zoom lens. Moreover, the Schlieren setup consisted of only one perspective, making it harder to correlate some flow structures. This can be addressed by setting up a dual Z-type Schlieren, forming a cross in the testing area to have a front view a side view. Despite all of these, some flow structures can be seen, such as the wing tip vortex (TV) and a vortex ring, as well as vortices shedding into the wake (Figure 3.5).

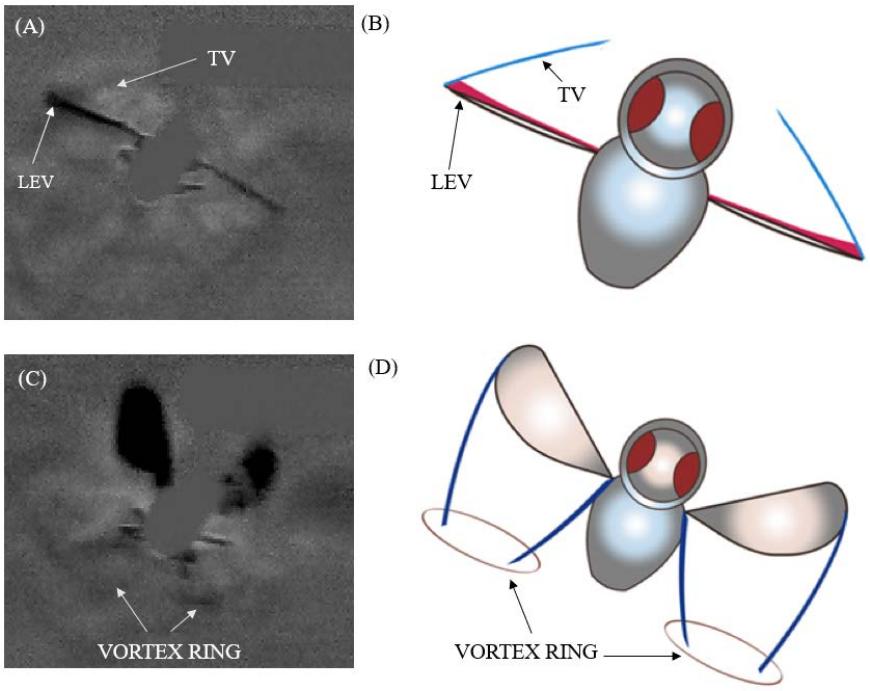

Figure 3.5 Vortex structures captured on a tethered house fly. (A & C) Images after background subtraction. (B & D) Illustration of the flow structures captured.

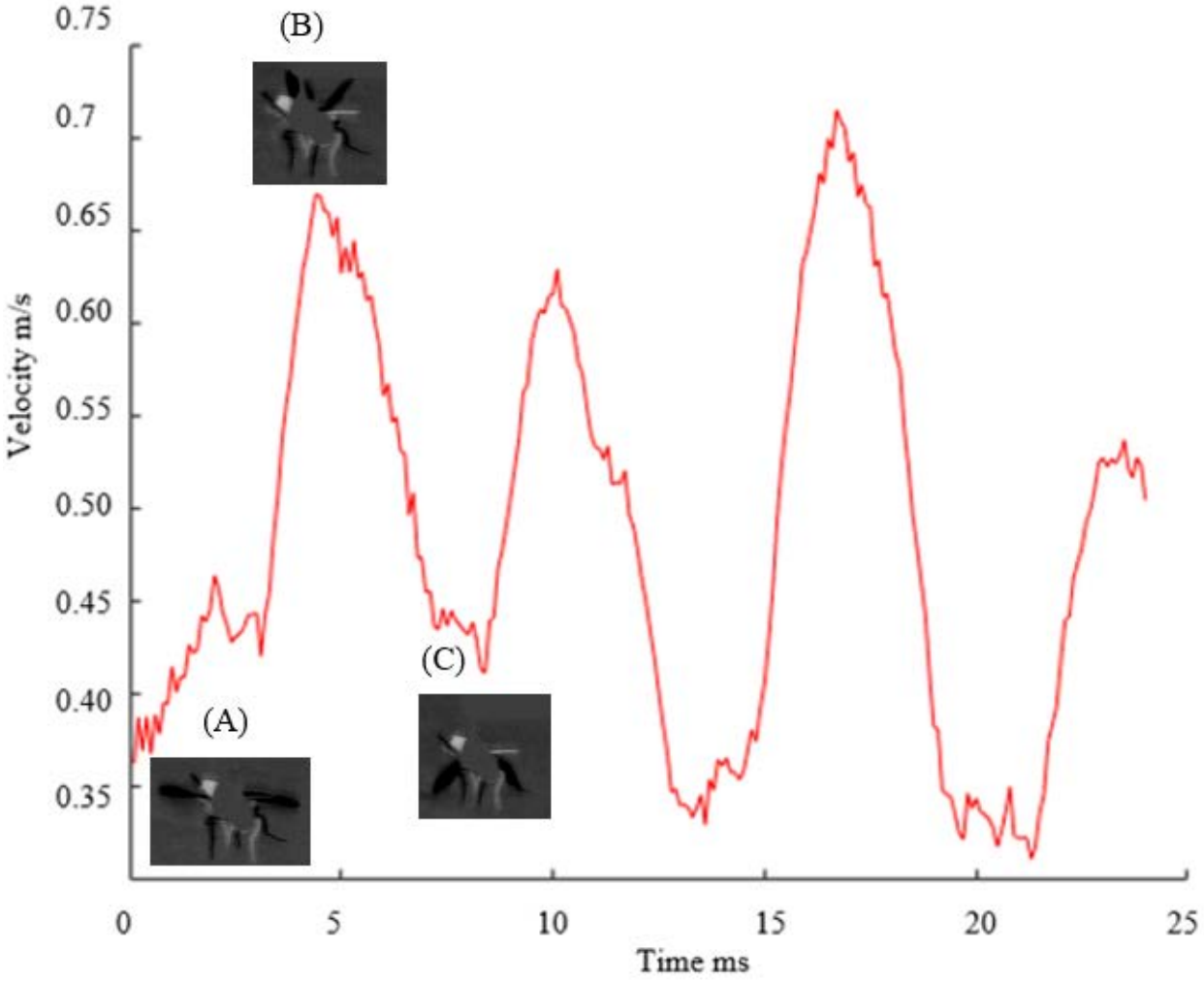

Figure 3. 6 Relationship between maximum velocity and wing location. (A) Wing position at time zero. (B) Wing position corresponding to the three peaks at 4.5, 10.1, and 16.7 ms. (C) Wing position at the three velocity drops corresponding to t = 8, 13.5, and 19.8 ms.

Due to the noisy images, the accuracy of the flow method is affected, and to handle this, a moving average was applied (similar to chapter two) to approximate the instantons velocity. Figure 3.6 is the moving average data where it can be seen a relationship between wing location during the stroke and maximum velocity. The three peaks located at t = 4.5, 10.1, and 16.7 correspond to the instant when the wings are fully extended upwards. On the other hand, velocity drop at t = 8, 13.5, and 19.8 correlates when the wings are fully extended downward. The reason to this can be seen in figure 3.7,a where can be seen a vortex ring shaded in the downstroke, entering the control volume (when wings are fully up). On the other hand, in figure 3.7.b (wings fully down), the vortex ring is dissipated, and velocity drops. Also, in figure 3.7,b,d, the contour

velocity matches the flow shape in figure 3.7,a,b. Moreover, the trend line showed in figure *3.6*, keeps a consistent pattern, demonstrating that the optical flow algorithm can be used to generate vector fields from Schlieren images.

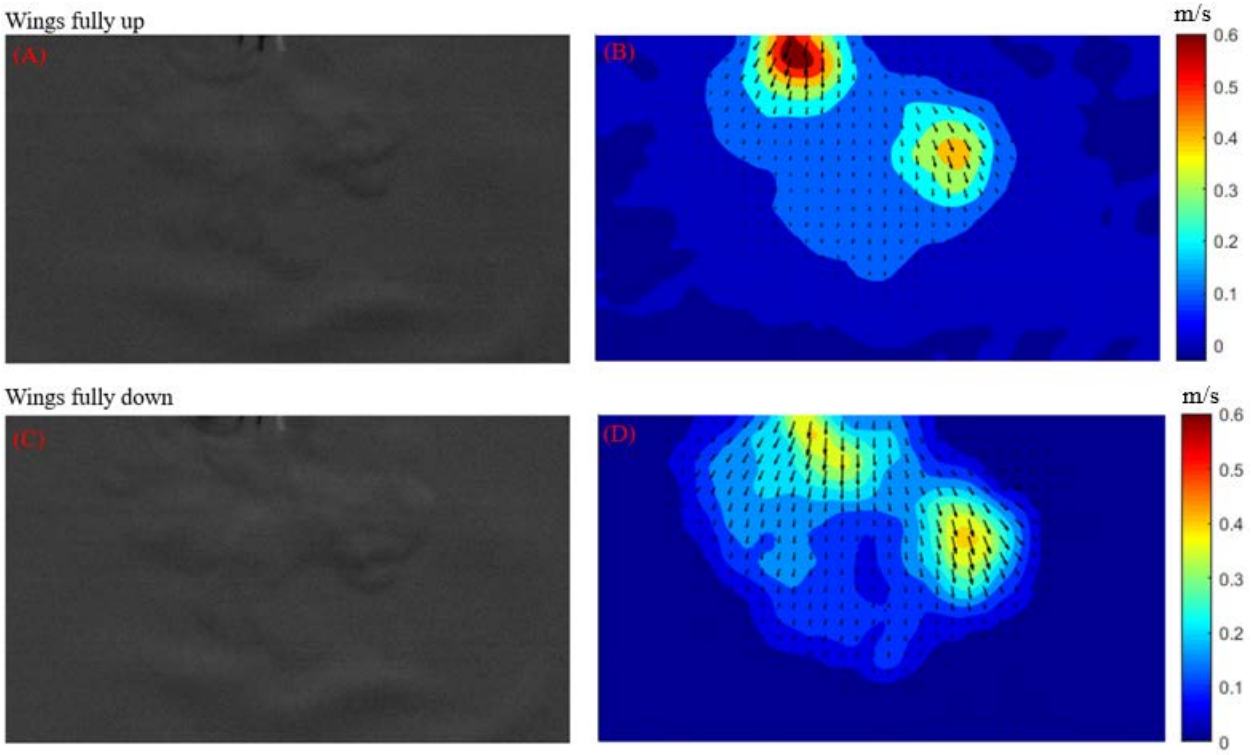

Figure 3. 7 Contour and velocity vector field when the wings are fully down and up. (A & B) The wings are fully up, and a vortex ring shed in the downstroke is entering the boundary. (C & D) The wings are pointing down, and the vortex is being dissipated.

The presented results are for a tethered housefly, but there is always uncertainty if the insect is really trying to fly or just moving the wings. Therefore, the best approach is to study a free-flying insect. For this reason, the same procedure was used to test if this approach can be used on free-flying houseflies. Similar to the tethered insect, there are some issues related to image noise; however, it was proven that it can be used to visualize the flow disturbed by the insect. The level of noise in the image in figure 3.8 is a little bit more than in the tethered housefly because it was used a 500 mm zoom lens. with the aim to visualize flow structures close to the wing better. As mentioned before, the noise level is related to the illumination of the images, a brighter point light source will fix this issue or record at a lower frame rate. However, the video has to be recorded at least at 4000 fps because a complete beat cycle is approximately

22-24 images at this frame rate. In figure 3.8 it is presented a free-flying housefly while it was turning to set on the optical glass. A preliminary estimation of the maximum velocity in y-direction was conducted. The maximum velocity at that particular instant was 0.57 m/s, demonstrating that this approach can be used to study free-flying insects.

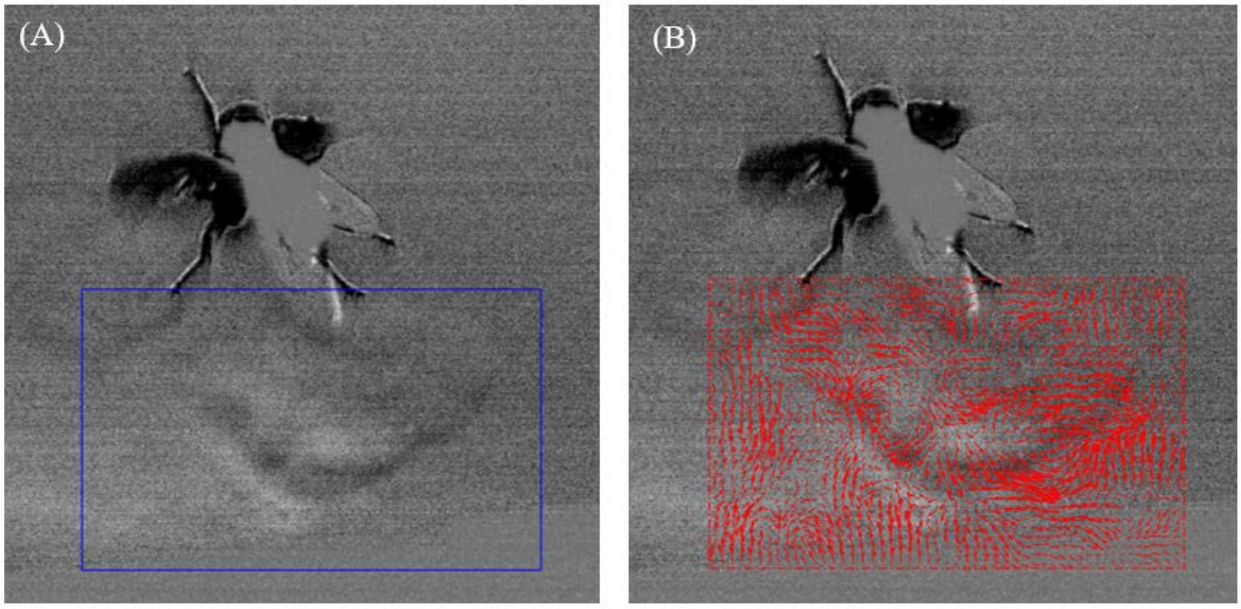

Figure 3. 8 (A) A fly turning 90 degrees to sit on the optical glass. (B) Vector velocity quantification at that particular instant. The maximum velocity inside the boundary was estimated to be 0.57 m/s.

3.4 Discussion

Combining Schlieren photography to visualize flow structures and using an optical flow method to quantify it opens a new door in insect aerodynamics studies. Studying small insects has been a challenge and limited to only CFD simulations or robotic scale model studies. As mentioned before, insect modeling is a very complex engineering task that requires wing kinematics tracking and replication of wing biological morphology. These models provide detailed information of vortices structures, but it requires validation of experimental studies. Moreover, PIV has been only used in few experiments to study a free-flying insect because it is challenging for an insect to behave naturally in the presence of a laser. Studying insects as they naturally behave can decipher hidden mechanisms that nature has found to optimize locomotion. For example, the Strouhal number of flying and swimming animals while cruise is in the range of 0.2 to 0.4. Suggesting this applies whether the propulsion of the animal is archived by the

wings or by the tail (Taylor, Nudds, & Thomas, 2003). Therefore, to fully understand the aerodynamic of insects, experimental data must be acquired from real insects while it is flying naturally. Although this chapter focused on a tethered house-fly, it can be seen in figure 3.9 that this approach can be used on a free-flying insect. Moreover, Schlieren is a non-intrusive method that allows studying animals in a natural setting, capturing all the vortices close and away from the insect body.

As mentioned before, noise in the images will reduce the accuracy of the optical flow method, and the most significant factor is the illumination. Due to insect wingbeat frequency increases as size decreases, a high-frame-rate camera is needed to study small insects. This is an issue as images get darker as the frame rate increases. Also, the size of the insect represents an issue because flow around the wings cannot be seen, and zooming is required, which also darkens the images. Moreover, taking into account that Schlieren photography needs to block light at the focal point to visualize changes in the index of refraction, this also impacts in overall illumination of the video and the image quality drop. Therefore, a powerful bright LED light source is required to avoid recording videos with noise and have constant illumination. Another issue discussed in this chapter is the number of perspectives to visualize the flow structures. This can be addressed by implementing two Z-type Schlieren setups forming a cross to view vortices from two different angles. Moreover, this can be used to reconstruct in 3D the vortex structures.

Also, flow visualization can be improved by increasing the temperature gradient inside the container. The temperature of the top is not recommended to get it higher since it is already at 35 ^{o}C and the flies start to slow down at 38 ^{o}C, and it is fatal beyond 45 ^{o}C (Keiding & Organization, 1986). Therefore, only the temperature at the bottom can be adjusted despite the fact that a fly is unable to fly at temperatures below 4 ^{o}C (Keiding & Organization, 1986). Currently, the cooling liquid is set at -5 ^{o}C but due to heat loss the temperature in the water block is 0 ^{o}C. The low temperature does not affect the fly performance of the insect because in this case of the tethered fly, the insect is placed almost at the top of the container and the insect is not affected by the low temperature. In the case of a free-flying insect, the insect will immediately start to fly to a higher location and will not be affected by the low temperature. This can also be used as a trick to motivate the insect to fly and record flow structures as the insect takes off. Therefore, lowering the temperature at the bottom and improving illumination will improve the flow signal and significantly reduce the noise in the images.

4. PRELIMINARY STUDY OF WAKE FLOW ON TETHERED HOUSE-FLY USING THE SHAKE-THE-BOX SYSTEM

4.1 Introduction

Three-dimensional measurement of velocity fields is a rapidly emerging field in experimental fluid mechanics. Depending on data extraction method, there are two types of 3D flow measurement techniques: 3D particle velocimetry (3D PTV) and Tomographic PIV (Schanz, Gesemann, & Schröder, 2016). Tomographic PIV has been used to study different kinds of flow phenomena, including biomedical flow, bio-locomotion, combustion, and turbulence. This method has been successfully implemented on a tethered locust, revealing the instantaneous three-dimensional vortex structures (Henningsson, et al., 2015). Despite the amazing details of the captured flow, the locust study was limited to flow reconstruction only in the far-field wake region. Moreover, it took 96 days to process all the data of a single beat cycle with a server with 48 cores and 64 GB of ram. Moreover, Tomographic PIV has issues at high-density seeding, which produces ghost particles that affect the resultant velocity vector (Schanz, Gesemann, & Schröder, 2016). Recent advancements in the Lagrangian particle tracking algorithm provide a novel solution to the 3D flow measurement. A new PTV algorithm of "Shake-the-Box" (STB) combines Iterative Particle Reconstruction (IPR) and an advanced 4D-PTV (Particle Tracking Velocimetry) that uses time information to track particles for reconstruction. The system uses spatial information from previous images to predict the future location of the particles in future time steps. The predicted particle location will be slightly off, and one method to fix this discrepancy is to move ("shake") the particle around space while exterminating the local residual (Schanz, Gesemann, & Schröder, 2016). Achieving high measurement accuracy of the flow with almost negligible ghost particle occurrence. Even though this method uses similar hardware as Tomographic-PIV. The Shake-the-Box system is much faster in processing the images, and it has a higher spatial resolution that can be increased to pixel level or below (Kähler, Scharnowski, & Cierpka, 2012). Usually, the "Shake-the-Box" computation time is 10 to 100 times less than for Tomographic-PIV. In this chapter some preliminary results on a tethered house fly with this method is presented.

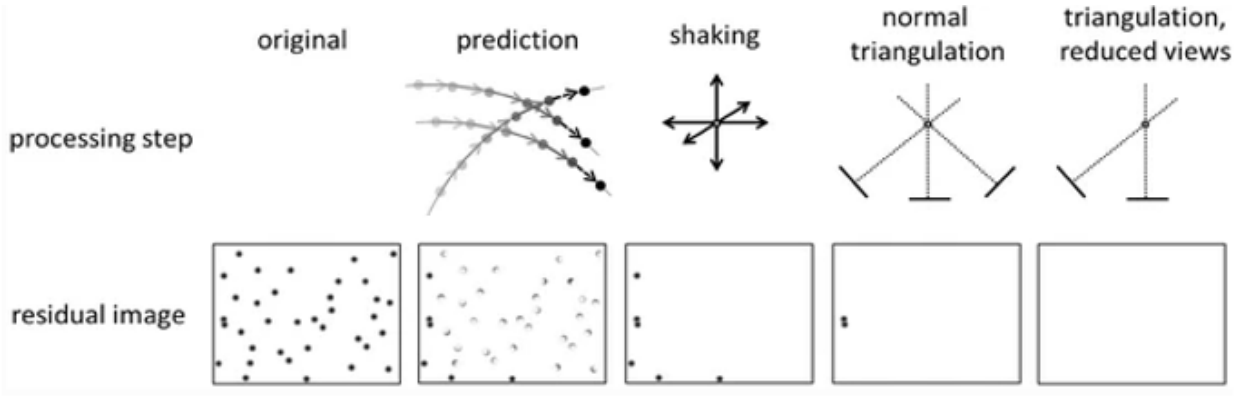

Figure 4. 1 Schematic of the different computational steps that the "Shake-the-Box" method uses to track particles. (Schanz, Gesemann, & Schröder, 2016)

4.2 Material and Methods

The state-of-the-art "Shake-the Box" system was used to resolve the complex flow field on a tethered housefly. The insect was tethered following the procedure described in chapter three. The system consisted of four consecutive high-speed and high-sensitivity cameras (Phantom 640L) and a high repetition rate laser (Nd:YLF single cavity Diode). The flow field is seeded by 1~5-**micron** fog particles (R700 Rockville Fog generator) that are illuminated by the laser, shot to 45^{o} inclined mirror on an optical table. The computer used for image processing consisted of a processor, Intel(R) Core (TM) i9-9940X @ 3.3 GHz with 64 GB of ram, and the software was LA VISION DAVIS.

To start the system's calibration, the laser was shot with a thickness of 6 mm to the mirror, and smoke was released. Then, the focus of each camera was adjusted to capture each particle perfectly. After this, a calibration target was placed in the testing area to gather illumination and spatial information for each camera. Combining the calibration target and a software tool helps to avoid human error in this critical step. Once the system was calibrated, the tethered housefly was placed in the testing area to start recording, similar to any PIV system procedure. The intensity of the laser was 34.00 A, and the image frame rate was 4.5 kHz. After this, the images were pre-processed, and a 3D volume was generated. For this step, the software package has an optical transfer function (OTF) that is used to characterize the shape and intensity of the particle within the volume. Finally, the images were processed with the "Shake-the-Box" algorithm to generate a 3D instantaneous particle tracking visualization. All of these took approximately 45 minutes to process 500 images.

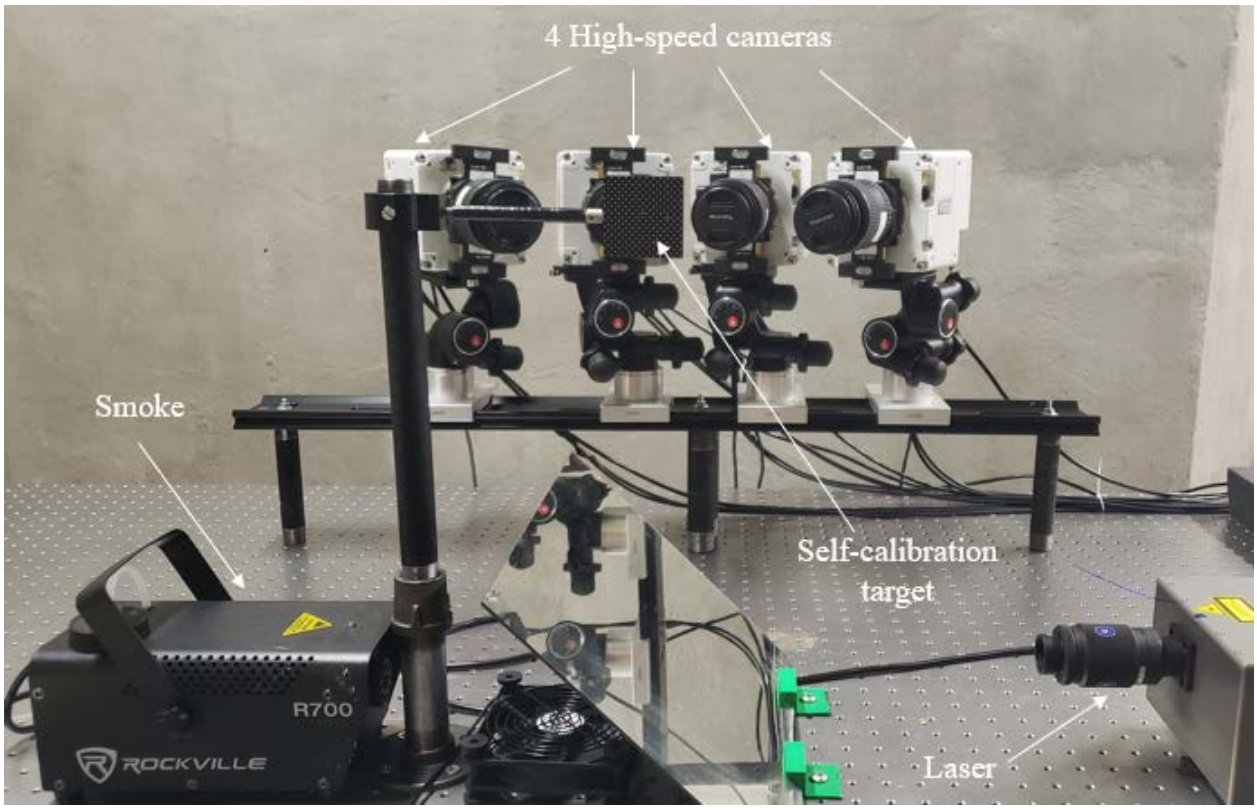

Figure 4. 2 Shake the box system setup. The calibration target is used to calibrate the system. Once the system is calibrated, it is replaced by a tethered insect.

4.3 Results

The preliminary results of the Lagrangian particle tracking “Shake-the-Box” system is presented in Figure 4.3 where the system was successfully implemented to measure the flow fields in the wake of a tethered housefly. The number of traced particles in the image is 5000 thousand, as a reference, 2000 is too little, and more than 8000 is too much. High seeding is definitely preferred since it can track small features, but too many results in convoluted flow measurement. Although, for flow visualization, this can be fixed by increasing the threshold of particle detection. It is worth mentioning that this amount of smokes particle is for studying a housefly; the STB algorithm can simultaneously track up to 275000 helium-filled soap bubbles (Huhn, et al., 2017).

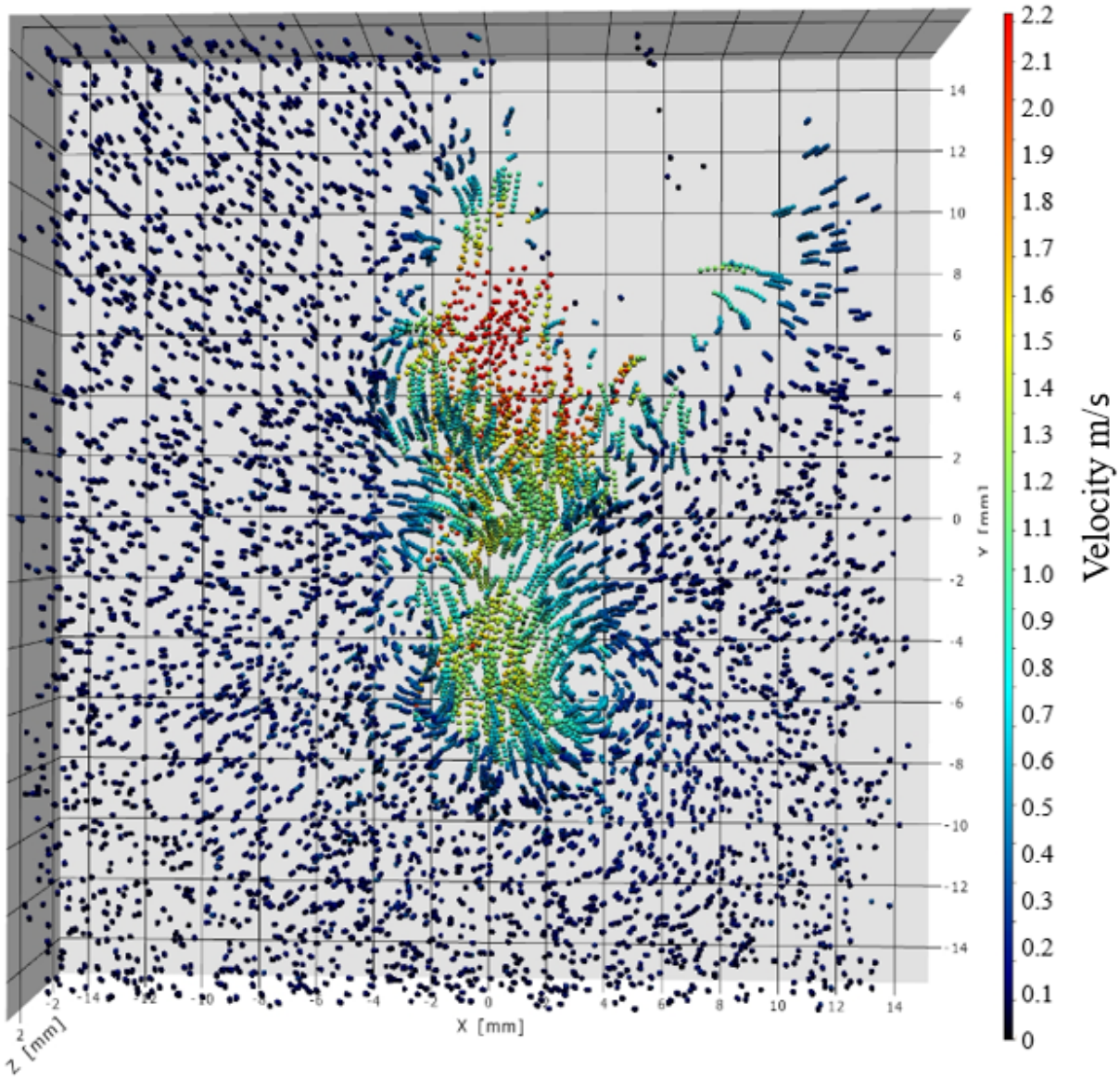

Figure 4. 3 Shake the box, individual traced particles on the wake of a tethered housefly.

The top right corner does not show traced particles because it is where the insect was placed to perform the experiment. This is a common issue in experiments involving animals due to seeding and light refraction caused by the animal body. This concatenates in poor particle reconstruction close to the wings, and the formation of vortices such as the LEV cannot be visualized. Despite this, the data acquired provides insight into the 3D flow motion of the vortices shed into the wake that cannot be obtained with 2D measurements. The figure shows the formation of two vortices due to the difference between the disturbed flow and the surrounding air. These vortices get entrained, and thanks to the 3D particle tracking, the interaction of the particle entering the vortex can be studied. Eulerian flow statistics are generated from the Lagrangian particle data using ensemble averaging with spatial bins (Godbersen &

Schröder, 2020). In addition, unlike traditional PIV parameters, velocity along the z-direction can be extracted, providing more details of flow phenomena. In figure 4.3 is presented the 3D velocity and vorticity field at the same time instant.

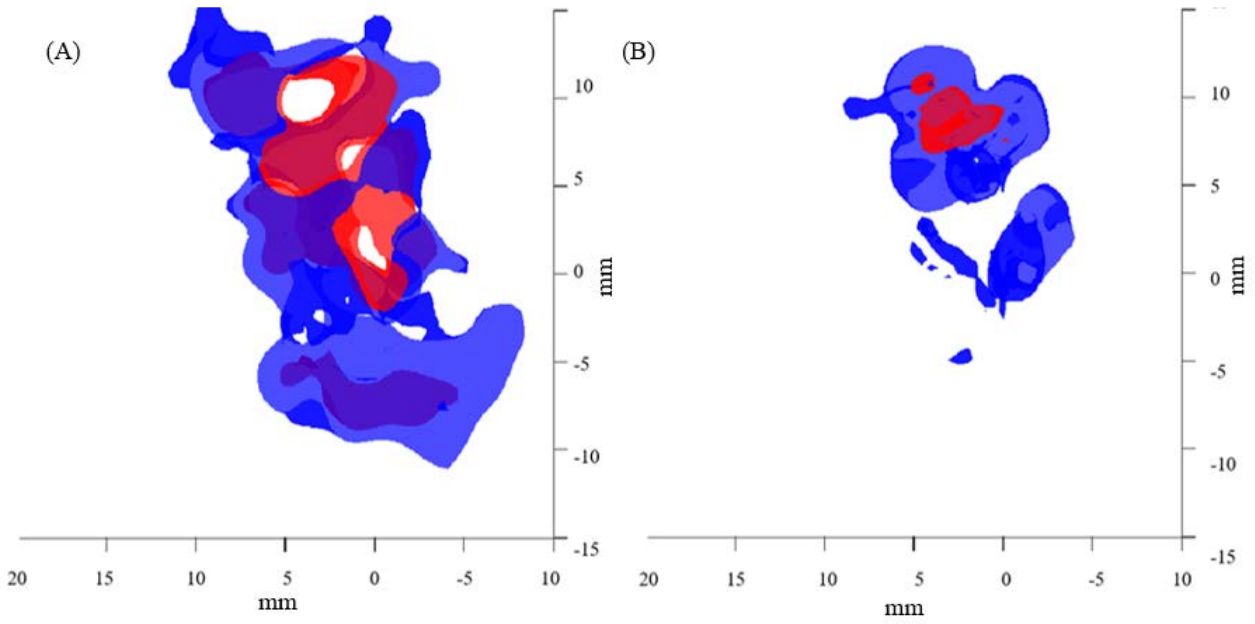

Figure 4. 3 (A & B) Isosurface plot of the velocity and vorticity at t = 0.02 ms respectevely. (A) Velocity. Red isosurface at 1 m/s and blue isosurface at 0.7 m/s. (B) Vorticity Red isosurface at 0.6 and blue isosurface at 0.3

4.4 Discussion

In the last decade, particle image velocimetry (PIV) has become a powerful tool in fluid mechanics studies, not only for 2D but also for 3D measurements. PIV resolution and accuracy have improved over the years. The “Shake-the-Box” system allows accurate measurement of each particle tracer's position, velocity, and acceleration. Thanks to implementing the self-calibration tool and calibration plate that avoids the human error of this critical step. In addition, the individual reconstruction of each particle provides instantaneous information at different z values that can be used to understand small insect aerodynamics better. As it was expected, vortices were generated by the wings in the shear layer due to Kelvin-Helmholtz's instabilities.

This chapter presents preliminary results for optimal settings to utilize the shake-the-box system to study a housefly. A laser sheet with a thickness of 6 mm at 34 A, and approximately 4000 smoke particles is currently adopted. This set a foundation of optimal settings for the

current setup to performed experiments in a housefly. However, some set-up modifications are currently being explored to track more particles closer to the wings. One approach is to set two cameras at both sides instead of using four consecutive cameras. Since some particles are not being reconstructed because they are only detected by one camera, there is not enough spatial information for a complete reconstruction of the particle trajectories. To measure the three components of the Lagrangian velocity, at least three different angles of view are required (Kasagi & Nishino, 1991). Therefore, another approach is to add more cameras to the setup to reduce the number of particles not detected for at least three cameras. Also, it was mentioned in chapter three, it is better to analyze data from a free-frying insect. For this reason, a way to carry out an experiment with a free-flying insect is being explored.

5. CONCLUSION

Millions of years of evolution have allowed insects and flying vertebrates to have the incredible aerial performance to travel vast distances and disperse around the world. Taking size into consideration, these animals can travel faster and reach higher altitudes than conventional aircraft. Therefore, it was natural to apply the well-established fixed-wing theories to analyze flapping wings, leading to the well-known paradox ‘bumblebee cannot fly’. In the past decades, this has inspired and gathered a lot of interest in the research community. Thanks to this, many hidden aerial mechanisms have been discovered, such as: added mass, rotational circulation, clap and fling, delayed stall, and wing–wake interactions. However, there is not a deep understating of flapping wings yet. Studying insect flight is a challenging problem that requires three-dimensional flow reconstruction and capturing flow structures close to the wings to understand the secrets behind their extraordinary aerial performance fully. This thesis explored two approaches to capture the vortex flow formation and evolution of a small insect (housefly).

The first approach was to use Schlieren photography to visualize flow phenomena of a tethered and a free-flying housefly using a vertical temperature-controlled gradient to induce changes in the index of refraction. Demonstrating the potential of Schlieren photography to capture vortex flow structures in the near and far-field of small insects. In addition, the Schlieren images were quantified using a physics-based optical flow method. This algorithm was pushed to its limits by analyzing two very complex flow phenomena. First, an unsteady and non-symmetric exit jet was studied using Schlieren photography, and the optical flow method was used to generate vector fields. The velocity profile, acceleration, and shear stress derivation match standard theories of jets. Demonstrating the applicability of this algorithm to quantify velocity fields from Schlieren images. On the other hand, in chapter three, the photos were noisy, and after applying some filters to enhance the photos, the optical flow estimations showed a low-velocity field compared with the velocity field of the shake-the-box. This can be attributed to the noise in the images and the fact that the experiments were conducted on two different insects. Despite this, as was shown in figure 3.7, the optical flow method was tracking the flow behavior. Therefore, this also confirms that code works with Schlieren images.

On the other hand, a state-of-the-art Lagrangian particle tracking technique was used to acquired preliminary results of a tethered housefly. Vortices formation was captured, and their

interaction with the surrounding environment was observed. However, since it is very complicated to capture flow structures near the wing with the “Shake-the-Box” system, but on the other hand, Schlieren is capable of doing that but cannot generate 3D measurements. It can be concluded that both methods can be used to complement each other and provide a better understanding of the formation and evolution of flow structures of insects.

REFERENCES

Adrian, R. J. (1991). Particle-Imaging Techniques for Experimental Fluid Mechanics. *Annual Review of Fluid Mechanics*, 261-394.

Aono, H., Liang, F., & Liu, H. (2008). Near- and far-field aerodynamics in insect hovering flight: an integrated computational study. Journal of Experimental Biology, 211, 239-257.

Benson, T. (2014). Combustion. NASA.

Benson, T. (2014). Match Stick Rocket. NASA.

Berg, C. v., & Ellington, C. P. (1997). The vortex wake of a 'hovering' model hawkmoth. The Royal Society B, 352(1351), 317-328.

Birch, J. M., Dickson, W. B., & Dickinson, M. H. (2004). Force production and flow structure of the leading edge vortex on flapping wings at high and low Reynolds numbers. Journal of Experimental Biology, 207, 1063-1072.

Bomphrey, R. J., Taylor, G. K., & Thomas, A. L. (2009). Smoke visualization of free-flying bumblebees indicates independent leading-edge vortices on each wing pair. Experiments in Fluids, 46, 811-821.

Chang, J., Zheng, S., Du, Y., Xu, J., Liu, Y., Guo, B., . . . Han, B. (2020). Investigation of Vortex Rings for Free Jet and Synthetic Jet at Various Reynolds Numbers and Strouhal Numbers. Mathematical Problems in Engineering.

Cheng, X., & Sun, M. (2016). Wing-kinematics measurement and aerodynamics in a small insect in hovering flight. Scientific Reports, 6(25706).

Chin, D. D., & Lentink, D. (2016). Flapping wing aerodynamics: from insects to vertebrates. Journal of Experimental Biology, 219, 920-932.

Corpetti, T., Mémin, É., & Pérez, P. (2002). Dense Estimation of Fluid Flows. IEEE Transactions on Pattern Analysis and Machine Intelligence , 365-380.

Dabiri, J. O. (2005). On the estimation of swimming and flying forces from wake measurements. Journal of Experimental Biology, 208, 3519-3532.

David, L., Jardin, T., & Farcy, A. (2009). On the non-intrusive evaluation of fluid forces with the momentum equation approach. Measurement Science and Technology, 20.

Davies, T. (1981). Schlieren photography - short bibliography and review. Optics & Laser Technology, 13(1), 37-42.

Dickinson, M. H., Lehmann, F.-O., & Sane, S. P. (1999). Wing Rotation and the Aerodynamic Basis of Insect Flight. Science, 284(5422), 1954-1960.

Douglas L. Altshuler, W. B., Vance, J. T., Roberts, S. P., & Dickinson, M. H. (2005). Short-amplitude high-frequency wing strokes determine the aerodynamics of honeybee flight. Proceedings of the National Academy of Sciences of the United States of America, 102, 18213-18218.

Duistermars, B. J., & Frye, M. A. (2008). A Magnetic Tether System to Investigate Visual and Olfactory Mediated Flight Control in Drosophila. Journal of Visualized Experiments, 21(1063).

Ellington, C. P. (1999). The novel aerodynamics of insect flight: applications to micro-air vehicles. Journal of Experimental Biology, 202, 3439-3448.

Ellington, C. P., Berg, C. v., Willmott, A. P., & Thomas, A. L. (1996). Leading-edge vortices in insect. Nature(384), 626-630.

Fry, S. N., Sayaman, R., & Dickinson, M. H. (2003). The Aerodynamics of Free-Flight Maneuvers in Drosophila. Science, 300(5618), 495-498.

Godbersen, P., & Schröder, A. (2020). Functional binning: improving convergence of Eulerian statistics from Lagrangian particle tracking. Measurement Science and Technology.

Gopal, V., Klosowiak, J. L., Jaeger, R., Selimkhanov, T., & Hartmann, M. J. (2008). Visualizing the invisible: the construction of three low-cost schlieren imaging systems for the undergraduate laboratory. European Journal of Physics, 29(3).

Gurstelle, W. (2012). Backyard Ballistics: Build Potato Cannons, Paper Match Rockets, Cincinnati Fire Kites, Tennis Ball Mortars, and More Dynamite Devices. Chicago Review Press.

Hall, N. (2015). Rocket Propulsion. NASA.

Hargather, M. J., Lawson, M. J., & Settles, G. S. (2011). Seedless Velocimetry Measurements by. AIAA Journal, 611-620.

Hedrick, T. L., Combes, S. A., & Miller, L. A. (2015). Recent developments in the study of insect flight. Canadian Journal of Zoology, 93(12), 925-943.

Heitz, D., Mémin, E., & Schnörr, C. (2009). Variational fluid flow measurements from image sequences: synopsis and perspectives. Experiments in Fluids, 369-393.

Henningsson, P., Michaelis, D., Nakata, T., Schanz, D., Geisle, R., Schröder, A., & Bomphrey, R. J. (2015). The complex aerodynamic footprint of desert locusts revealed by large-volume tomographic particle image velocimetry. Journal of The Royal Society Interface, 12(108).

Horn, B. K., & G.Schunck, B. (1981). Determining optical flow. Artificial Intelligence, 185-203.

Huhn, F., Schanz, D., Gesemann, S., Dierksheide, U., Meerendonk, R. v., & Schröder, A. (2017). Large-scale volumetric flow measurement in a pure thermal plume by dense tracking of helium-filled soap bubbles. Experiments in Fluids .

Jardin, T., Chatellier, L., Farcy, A., & David, L. (2009). Correlation between vortex structures and unsteady loads for flapping motion in hover. Experiments in Fluids, 47.

Kähler, C. J., Scharnowski, S., & Cierpka, C. (2012). On the resolution limit of digital particle image velocimetry. Experiments in Fluids, 52, 1629-1639.

Kasagi, N., & Nishino, K. (1991). Probing turbulence with three-dimensional particle-tracking velocimetry. Experimental Thermal and Fluid Science, 601-612.

Keiding, J., & Organization, W. H. (1986). The house-fly : biology and control. Denmark: Division of Vector Biology and Control.

Kmecova, M., Sikula, O., & Krajcik, M. (2019). Circular Free Jets: CFD Simulations with Various Turbulence Models and Their Comparison with Theoretical Solutions. IOP Conference Series: Materials Science and Engineering.

Lehmann, F.-O. (2012). Wake Structure and Vortex Development in Flight of Fruit Flies Using High-Speed Particle Image Velocimetry. Nature-inspired Fluid Mechanics, 119, 65-80.

Lehmann, F.-O., Sane, S. P., & Dickinson, M. (2005). The aerodynamic effects of wing–wing interaction in flapping insect wings. Journal of Experimental Biology, 3075-3092.

Liu, H. (2009). Integrated modeling of insect flight: From morphology, kinematics to aerodynamics. Journal of Computational Physics(228), 439-459.

Liu, H., & Aono, H. (2009). Size effects on insect hovering aerodynamics: an integrated computational study. Bioinspiration & Biomimetics, 4.

Liu, H., Ravi, S., Kolomenskiy, D., & Tanaka, H. (2016). Biomechanics and biomimetics in insect-inspired flight systems. Philosophical Transactions of the Royal Society B, 371(1704).

Liu, T., & Shen, L. (2008). Fluid flow and optical flow. Journal of Fluid Mechanics, 614, 253-291.

Liu, Y., Roll, J., Kooten, S. V., & Deng, X. (2018). Schlieren photography on freely flying hawkmoth. Journal of The Royal Society Biology Letters, 14(5).

Mazumdar, A. (2013). Principles and Techniques of Schlieren Imaging Systems. New York: Columbia University.

McMasters, J. H. (1989). The Flight of the Bumblebee and Related Myths of Entomological Engineering: Bees help bridge the gap between science and engineering. American Scientist, 77(2), 164-1989.

Mohamed, M. N., Sivapirakasam, S., & Surianarayanan, M. (2013). Experimental investigation on the impact sensitivity of a match head composition influenced by the surface roughness of in-process contact materials. Process Safety and Environmental Protection, 91(5), 343-350.

Muijres, F. T., Johansson, L. C., Barfield, R., Wolf, M., Spedding, G. R., & Hedenström, A. (2008). Leading-Edge Vortex Improves Lift in. Science, 319, 1250-1253.

Nabawy, M. R., & Crowther, W. J. (2017). The role of the leading edge vortex in lift augmentation of steadily revolving wings: a change in perspective. Journal of the Royal Society Interface .

Nations, J. C. (1988). NASA/Aerospace Education Services Program. Classroom Activities.

Oh, S., Lee, B., Park, H., Choi, H., & Kim, S.-T. (2019). A numerical and theoretical study of the aerodynamic performance of a hovering rhinoceros beetle (Trypoxylus dichotomus). Journal of Fluid Mechanics, 885.

Ray, N. (2011). Computation of Fluid and Particle Motion From a Time-Sequenced Image Pair: A Global Outlier Identification Approach. IEEE Trans Image Process.

Ruhnau, P., Kohlberger, T., Schnörr, C., & Nobach, H. (2005). Variational optical flow estimation for particle image velocimetry. Experiments in Fluids, 21-32.

Sane, S. P. (2003). The aerodynamics of insect flight. The Journal of Experimental Biology , 206, 4191-4208.

Schanz, D., Gesemann, S., & Schröder, A. (2016). Shake-The-Box: Lagrangian particle tracking at high particle image densities. Experiments in Fluids, 57(70).

Settles, G. (2001). Schlieren and Shadowgraph Techniques: Visualizing Phenomena in Transparent Media. Berlin: Springer.

Sforzini, R. H. (1970). Derivation of the Thrust Equation from Conservation of Energy. Journal of Aircraft, 7(6), 538-541.

Taberlet, N., Plihon, N., Auzémery, L., Sautel, J., Panel, G., & Gibaud, T. (2018). Synthetic schlieren—application to the visualization and characterization of air convection. European Journal of Physics, 39(3).

Taylor, G. K., Nudds, R. L., & Thomas, A. L. (2003). Flying and swimming animals cruise at a Strouhal number tuned for high power efficiency. Nature, 707-711.

Townend, H. C. (1936). A Method of Air Flow Cinematography Capable of Quantitative Analysis. Journal of the Aeronautical Science, 342-352.

Traldi, E., Boselli, M., Simoncelli, E., Stancampiano, A., Gherardi, M., Colombo, V., & Settle, G. S. (2018). Schlieren imaging: a powerful tool for atmospheric plasma diagnostic. EPJ Techniques and Instrumentation volume, 5.

Truong, T. V., Nguyen, Q.-V., & Lee, H. P. (2017). Bio-Inspired Flexible Flapping Wings with Elastic Deformation. Aerospace.

Usherwood, J. R., & Ellington, C. P. (2002). The aerodynamics of revolving wings II. Propeller force coefficients from mayfly to quai. Journal of Experimental Biology , 1565-1576.

Veldhuis, C., Biesheuvel, A., Wijngaarden, L. v., & Lohse, D. (2004). Motion and wake structure of spherical particles. Nonlinearity, 18.

Walker, S. M., Thomas, A. L., & Taylor, G. K. (2009). Deformable wing kinematics in free-flying hoverflies. Journal of The Royal Society Interface, 7(42), 131-142.

Wang, Z. J. (2005). Dissecting Insect Flight. Annual Review of Fluid Mechanics, 183-210.

Weinstein, L. (2010). Review and update of lens and grid schlieren and motion camera schlieren. The European Physical Journal Special Topics , 182, 65-95.

PRESENTATIONS AND PUBLICATIONS

1. Y Liu, C Li, **A Lozano**. Vortex structure comparison between experimental and computational studies on a hovering hawkmoth. *73rd Annual Meeting of the APS Divisions of Fluid Dynamics,* Nov 22-24, 2020; Virtual

2. **A Lozano**, Y Liu. High speed schlieren photography on match rockets (Gallery of Fluid Motion). 73rd Annual Meeting of the APS Divisions of Fluid Dynamics, Nov 22-24, 2020; Virtual

3. **A Lozano**, Y Liu. High speed schlieren photography on small insects. 72nd Annual Meeting of the APS Divisions of Fluid Dynamics, Nov 23-26, 2019; Seattle, Washington

4. Y Liu, **A Lozano**, T Hedrick, C Li. Comparison of Experimental and Numerical Studies on the Flow Structures of Hovering Hawkmoths. Under Review